Inorg. Chem. **2006**, *45*, 10537–10551

Structural and Magnetic Diversity in Cyano-Bridged Bi- and Trimetallic Complexes Assembled from Cyanometalates and [M(*rac*-CTH)]$^{n+}$ Building Blocks (CTH = *d,l*-5,5,7,12,12,14-Hexamethyl-1,4,8,11-tetraazacyclotetradecane)

Antonio Rodríguez-Diéguez,[†] Raikko Kivekäs,[‡] Reijo Sillanpää,[§] Joan Cano,[∥] Francesc Lloret,[⊥] Vickie McKee,[#] Helen Stoeckli-Evans,[⊗] and Enrique Colacio*,[†]

Departamento de Química Inorgánica, Facultad de Ciencias, Universidad de Granada, 18071 Granada, Spain, Department of Chemistry, Laboratory of Inorganic Chemistry, P.O. Box 55, FIN-00014 University of Helsinki, Finland, Department of Chemistry, University of Jyväskylä, FIN-40351 Jyväskylä, Finland, Departament de Química Inorgànica and Centre de Recerca en Química Teórica, Institució Catalana de Recerca i Estudis Avançats (ICREA), Universitat de Barcelona, Av. Diagonal 647, 08027 Barcelona, Spain, Departament de Química Inorgánica/ Instituto de Ciencia Molecular, Facultat de Ciencias, Universitat de Valencia, Avda. Dr. Moliner 50, 46100 Burjassot, Valencia, Spain, Chemistry Department, Loughborough University, Loughborough, Leicestershire LE11 3TU, U.K., and Institut de Chimie, Université de Neuchâtel, Avenue de Bellevaux 51, CH-2000 Neuchâtel, Switzerland

Received June 29, 2006

Seven new cyano-bridged heterometallic systems have been prepared by assembling [M′(*rac*-CTH)]$^{n+}$ complexes (M′ = Cr^{III}, Ni^{II}, Cu^{II}), which have two cis available coordination positions, and [M(CN)$_6$]$^{3-}$ (M = Fe^{III}, Cr^{III}) and [Fe(CN)$_2$(bpy)$_2$]$^+$ cyanometalate building blocks. The assembled systems, which have been characterized by X-ray crystallography and magnetic investigations, are the molecular squares (*meso*-CTH-H$_2$)[{Ni(*rac*-CTH)}$_2${Fe(CN)$_6$)}$_2$]·5H$_2$O (**2**) and [{Ni(*rac*-CTH)}$_2${Fe(CN)$_2$(bpy)$_2$}$_2$](ClO$_4$)$_4$·H$_2$O (**5**), the bimetallic chain [{Ni(*rac*-CTH)}$_2${Cr(CN)$_6$)}$_2$Ni(*meso*-CTH)]·4H$_2$O (**3**), the trimetallic chain [{Ni(*rac*-CTH)}$_2${Fe(CN)$_6$)}$_2$Cu(cyclam)]·6H$_2$O (**4**), the pentanuclear complexes [{Cu(*rac*-CTH)}$_3${Fe(CN)$_6$)}$_2$]·2H$_2$O (**6**) and [{Cu(*rac*-CTH)}$_3${Cr(CN)$_6$)}$_2$]·2H$_2$O (**7**), and the dinuclear complex [Cr(*rac*-CTH)(H$_2$O)Fe(CN)$_6$]·2H$_2$O (**8**). With the exception of **5**, all compounds exhibit ferromagnetic interaction between the metal ions (J_{FeNi} = 12.8(2) cm^{-1} for **2**; J_{1FeCu}= 13.8(2) cm^{-1} and J_{2FeCu}= 3.9(4) cm^{-1} for **6**; J_{1CrCu}= 6.95(3) cm^{-1} and J_{2CrCu}= 1.9(2)cm^{-1} for **7**; J_{CrFe} = 28.87(3) cm^{-1} for **8**). Compound **5** exhibits the end of a transition from the high-spin to the low-spin state of the octahedral Fe^{II} ions. The bimetallic chain **3** behaves as a metamagnet with a critical field H_c = 300 G, which is associated with the occurrence of week antiferromagnetic interactions between the chains. Although the trimetallic chain **4** shows some degree of spin correlation along the chain, magnetic ordering does not occur. The sign and magnitude of the magnetic exchange interaction between Cr^{III} and Fe^{III} in compound **8** have been justified by DFT type calculations.

Introduction

In recent years, much research effort has been devoted to the synthesis and characterization of multidimensional cyano-bridged metal complexes.[1] The most common and controlled strategy to prepare this kind of system consists of the self-assembly of specifically designed precursors, typically a cyanometalate complex that acts as a ligand and a transition metal complex with free or available coordination sites for the nitrogen atoms of the cyanide groups. Thus, the reaction between hexacyanometalate anions [M′(CN)$_6$]$^{3-}$ and fully solvated metal ions, [M(S)$_6$]$^{2+}$ (S = solvent), leads to the well-known family of bimetallic Prussian blue analogues, which possess a fcc 3D structure and exhibit interesting properties, such as high-T_c molecule-based magnetism,[1k] photo-,[2] electro-,[3] and piezomagnetism,[4] hydrogen storage,[5]

* To whom correspondence should be addressed. E-mail: ecolacio@ugr.es. Phone: 0034-958243236.
[†] Universidad de Granada.
[‡] University of Helsinki.
[§] University of Jyväskylä.
[∥] Universitat de Barcelona.
[⊥] Universitat de Valencia.
[#] Loughborough University.
[⊗] Université de Neuchâtel.

10.1021/ic061187j CCC: $33.50
Published on Web 11/16/2006

biosensors,[6] host−guest chemistry,[7] nanosized magnetic materials,[8] etc. The crystallization of the Prussian-blue analogues, however, is very difficult, and therefore, structural information is very limited.[9] More crystalline bimetallic compounds with reduced dimensionality can be obtained by using polydentate end-cap ligands that block some metal coordination positions (either on M or M′) and restrict the spatial extension of the structure. Following this route, a great variety of cyano-bridged bimetallic compounds have been prepared, which are playing an important role in areas such as high-T_c magnetic materials,[10] photoinduced magnetism,[11] spin-crossover (SCO) materials,[12] host−guest chemistry,[13] vapochromic materials,[14] magnetochirality,[15] etc. Among these systems, those exhibiting very slow relaxation of their magnetization, such as anisotropic large-spin paramagnetic molecules that behave as SMM (single-molecule magnets)[16] and large-spin anisotropic well-isolated 1D systems that behave as SCM (single-chain magnets),[17] are of particular research interest. For instance, it has been recently shown that cyano-bridged $Fe^{III}_2Ni^{II}_2$ (molecular square),[16b] $Fe^{III}_2Ni^{II}$ (bent),[16c] $Mn^{III}_6Fe^{III}_6$ (molecular wheel),[16f] $Mn^{II}Cr^{III}_6$ (trigonal prismatic),[16e] $Mn^{II}_2Mn^{III}_2$ (bpyramidal trigonal),[16d] and Mn^{III}_3-Fe^{III} (T-shaped)[16g] clusters exhibit SMM behavior, whereas cyano-bridged Fe/Mn,[17c] Fe/Co,[17a,b] and Fe/Cu[17d] bimetallic chains show SCM behavior. The dimensionality and topology of these assemblies strongly depends on the nature of ML_x (number and disposition of empty or available coordination positions on M, coordination geometry, volume of the ligands, etc.) and the connectivity of the cyanometalate building block (number and arrangement of ML_x units around M′). It should be noted that the assembly of coordinatively unsaturated ML_x metal complexes having two available cis coordination positions and cyanometalates has been shown to be particularly fruitful in the preparation of high-nuclearity

(1) Some reviews: (a) Dunbar, K. R.; Heintz, R. A. *Prog. Inorg. Chem.* **1997**, *45*, 283. (b) Verdaguer, M. *Science* **1996**, *272*, 698. (c) Verdaguer, M.; Bleuzen, A.; Marvaud, V.; Vaissermann, J.; Seuleiman, M.; Desplanches, C.; Scuiller, A.; Train, C.; Garde, R.; Gelly, G.; Lomenech, C.; Rosenman, I.; Veillet, P.; Cartier, C.; Villain, F. *Coord. Chem. Rev.* **1999**, *190*, 1023. (d) Fehlhammer, W. P.; Fritz, M. *Chem. Rev.* **1993**, *93*, 1243. (e) Ohba, M.; Okawa, K. *Coord. Chem. Rev.* **2000**, *198*, 313. (f) Èernák, J.; Orendáè, M.; Potoèòák, I.; Chomiè, J.; Orendáèová, A.; Skoršepa, J.; Feher, A. *Coord. Chem. Rev.* **2002**, *224*, 51 and references therein. (g) Chesnut, D. J.; Hagrman, D.; Zapf, P. J.; Hammond, R. P.; LaDuca, R.; Haushalter, R. C.; Zubieta, J. *Coord. Chem. Rev.* **1999**, *190*, 737 and references therein. (g) Miller, J. S.; Manson, J. L. *Acc. Chem. Res.* **2001**, *34*, 563. (h) Rogez, G.; Rivière, E.; Mallah, T. *C. R. Chimie* **2003**, *6*, 283. (i) Pilkington, M.; Decurtins, S. In *Comprehensive Coordination Chemistry II. From Biology to Nanaotechnology*; MacCleverty, J. A., Meyer, T. J., Eds.; Elsevier: Amsterdam, 2004; Vol. 7, p 177. (j) Pilkington, M.; Decurtins, S. *Perspect. Supramol. Chem.* **2003**, *7*, 275. (k) Beltran, L. M.; Long, J. R. *Acc. Chem. Res.* **2005**, *38*, 325. (l) Verdaguer, M.; Girolami, G. In *Magnetism: Molecules to Materials*; Miller, J. S., Drillon, M., Eds.; Wiley-VCH: Weinheim, Germany, 2005; Vol. 5, p 283 and references therein.

(2) (a) Sato, O.; Iyoda, T.; Fujishima, A.; Hashimoto, K. *Science* **1996**, *272*, 704. (b) Sato, O. *Acc. Chem. Res.* **2003**, *36*, 692 and references therein. (c) Sato, O.; Einaga, Y.; Fujishima, A.; Hashimoto, K. *Inorg. Chem.* **1999**, *38*, 4405. (d) Bleuzen, A.; Lomenech, C.; Escax, V.; Villain, F.; Varret, F.; Cartier dit Moulin, C.; Verdaguer, M. *J. Am. Chem. Soc.* **2000**, *122*, 6648. (e) Escax, V.; Bleuzen, A.; Cartier dit Moulin, C.; Villain, F.; Goujon, A.; Varret, F.; Verdaguer, M. *J. Am. Chem. Soc.* **2001**, *123*, 12536. (f) Hozumi, T.; Hashimoto, K.; Ohkoshi, S. *J. Am. Chem. Soc.* **2005**, *127*, 3864. (g) Catala, L.; Mathoniere, C.; Gloter, A.; Stephan, O.; Gacoin, T.; Boilot, J. P.; Mallah, T. *Chem. Commun.* **2005**, *6*, 746. (h) Ohkoshi, S. I.; Tokoro, H.; Hozumi, T.; Zhang, Y.; Hashimoto, K.; Mathoniere, C.; Bord, I.; Rombaut, G.; Verelst, M.; Cartier dit Moulin, C.; Villain, F. *J. Am. Chem. Soc.* **2006**, *128*, 270.

(3) Sato, O.; Yyoda, T.; Fujishima, A.; Hashimoto, K. *Science* **1996**, *271*, 49.

(4) Coronado, E.; Giménez-López, M. C.; Levchenko, G.; Romero, F. M.; García-Baonza, V.; Milner, A.; Paz-Pasternak, M. *J. Am. Chem. Soc.* **2005**, *127*, 4580.

(5) Kaye, S. S.; Long, J. R. *J. Am. Chem. Soc.* **2005**, *127*, 6506.

(6) Ricci, F.; Paleschi, G. *Biosens. Bioelectron.* **2005**, *21*, 389.

(7) Iwamoto, T. *J. Inclusion Phenom. Mol. Recognit. Chem.* **1996**, *24*, 61.

(8) See for example: (a) Taguchi, M.; Yamada, K.; Suzuki, K.; Sato, O.; Einaga, Y. *Chem. Mater.* **2005**, *17*, 4554. (b) Dominguez-Vera, J. M.; Colacio, E. *Inorg. Chem.* **2003**, *42*, 6983.

(9) (a) Dong, W.; Zhu, L.-N.; Song, H.-B.; Liao, D.-Z.; Jiang, Z.-H.; Yan, S.-P.; Cheng, P.; Gao, S. *Inorg. Chem.* **2004**, *43*, 2465. (b) Zhou, H.-B.; Zhang, W.; Yoshimura, K.; Ouyang, Y.; Liao, D.-Z.; Jiang, Z.-H.; Yan, S.-P.; Cheng, P. *Chem. Commun.* **2005**, *39*, 4979. (c) Franz, P.; Ambrus, C.; Hauser, A.; Chernyshov, D.; Hostettler, M.; Hauser, J.; Keller, L.; Kraemer, K.; Stoeckli-Evans, H.; Pattison, P.; Buergi, H.-B.; Decurtins, S. *J. Am. Chem. Soc.* **2004**, *126*, 16472. (d) Kumar, A.; Yusuf, S. M.; Keller, L. *Phys. Rev. B* **2005**, *71*, 54414/1.

(10) (a) Kou, H.; Gao, S.; Zhang, J.; Su, G.-H.; Zheng, R. K.; Zhang, X. X. *J. Am. Chem. Soc.* **2001**, *123*, 11809. (b) Ohba, M.; Usuki, N.; Fukita, N.; Okawa, H. *Angew. Chem.* **1999**, *111*, 1911; *Angew. Chem., Int. Ed.* **1999**, *38*, 1795. (c) Tanase, S.; Tuna, F.; Guionneau, P.; Maris, T.; Rombaut, G.; Mathionière, C.; Andruh, M.; Khan, O.; Sutter, J. P. *Inorg. Chem.* **2003**, *42*, 1625.

(11) (a) Rombaut, G.; Golhen, S.; Ouahab, L.; Mathoniere, C.; Kahn, O. *J. Chem. Soc., Dalton Trans.* **2000**, *20*, 3609. (b) Arimoto, Y.; Ohkoshi, S. I.; Zhong, Z. J.; Seino, H.; Mizobe, Y.; Hashimoto, K. *J. Am. Chem. Soc.* **2003**, *125*, 9240. (c) Mathoniere, C.; Podgajny, R.; Guionneau, P.; Labrugere, C.; Sieklucka, B. *Chem. Mater.* **2005**, *17*, 442. (d) Herrera, J. M.; Marvaud, V.; Verdaguer, M.; Marrot, J.; Kalisz, M.; Mathoniere, C. *Angew. Chem.* **2004**, *116*, 5584; *Angew. Chem., Int. Ed.* **2004**, *43*, 5468.

(12) (a) Real, J. A.; Gaspar, A. B.; Niel, V.; Muñoz, M. C. *Coord. Chem. Rev.* **2003**, *236*, 121. (b) Galet, A.; Niel, V.; Muñoz, M. C.; Real, J. A. *J. Am. Chem. Soc.* **2003**, *125*, 14224. (c) García, Y.; Niel, V.; Muñoz, M. C.; Real, J. A. *Top. Curr. Chem.* **2004**, *233*, 229. (d) Niel, V.; Thompson, A. L.; Goeta, A. E.; Enachescu, C.; Hauser, A.; Galet, A.; Munoz, M. C.; Real, J. A. *Chemistry* **2005**, *11*, 2047. (e) Berlinguette, C. P.; Dragulescu-Andrasi, A.; Sieber, A.; Galán-Mascarós, J. R.; Güdel, H.-U.; Achim, C.; Dunbar, K. R. *J. Am. Chem. Soc.* **2004**, *126*, 6222.

(13) (a) Ibrahim, M. S.; Werida, A.; Etaiw, S. *Phosphorus, Sulfur Silicon Relat. Elem.* **2004**, *179*, 2441. (b) Yoshikawa, H.; Nishikiori, S. *Dalton Trans.* **2005**, *18*, 3056. (c) Yang, J. Y.; Shores, M. P.; Sokol, J. J.; Long, J. R. *Inorg. Chem.* **2003**, *42*, 1403.

(14) Lefebvre Julie, J.; Batchelor, R. J.; Leznoff, D. B. *J. Am. Chem. Soc.* **2004**, *126*, 16117.

(15) (a) Inoue, K.; Ohkoshi, S.; Imai, H. *Magnetism: Molecules to Materials*; Miller, J. S., Drillon, M., Eds.; Wiley-VCH: Weinheim, Germany, 2005; Vol. 5, p 41 and references therein. (b) Coronado, E.; Giménez-Saiz, C.; Martínez-Agudo, J. M.; Nuez, A.; Romero, F. M.; Stoeckli-Evans, H. *Polyhedron* **2003**, *22*, 2435. (c) Imai, H.; Inoue, K.; Kikuchi, K.; Yoshida, Y.; Ito, M.; Sunahara, T.; Onaka, S. *Angew. Chem., Int. Ed.* **2004**, *43*, 5618.

(16) (a) Wang, S.; Zuo, J. L.; Zhou, H. C.; Choi, H. J.; Ke, Y.; Long, J. R.; You, X. Z. *Angew. Chem., Int. Ed.* **2004**, *43*, 5940. (b) Li, D.; Parkin, S.; Wang, G.; Yee, G. T.; Prosvirin, A. V.; Holmes, S. M. *Inorg. Chem.* **2005**, *44*, 4903. (c) Li, D.; Clérac, R.; Parkin, S.; Wang, G.; Yee, G. T.; Holmes, S. M. *Inorg. Chem.* **2006**, *45*, 5251. (d) Berlinguette, C. P.; Vaughn, D.; Cañada-Vilalta, C.; Galán-Mascarós, J. R.; Dunbar, K. R. *Angew. Chem., Int. Ed.* **2003**, *42*, 1523. (e) Sokol, J. J.; Hee, A. G.; Long, J. R. *J. Am. Chem. Soc.* **2002**, *124*, 7656. (f) Ni, Z.-H.; Kou, H.-Z.; Zhang, L.-F.; Ge, C.; Cui, A.-L.; Wang, R.-J.; Li, Y.; Sato, O. *Angew. Chem., Int. Ed.* **2005**, *44*, 7742. (g) Misayaka, H.; Takahashi, H,; Madanbashi, T.; Sugiura, K.; Clérac, R.; Nojori, H. *Inorg. Chem.* **2005**, *44*, 5969.

(17) (a) Lescouëzec, R.; Vaissermann, J.; Ruiz-Pérez, C.; Lloret, F.; Carrasco, R.; Julve, M.; Verdaguer, M.; Dromzée, Y.; Gatteschi, D.; Wernsdorfer, W. *Angew. Chem., Int. Ed.* **2003**, *42*, 1483. (b) Toma, M. L.; Lescouëzec, R.; Lloret, F.; Julve, M.; Vaissermann, J.; Verdaguer, M. *Chem. Commun.* **2003**, *15*, 1850. (c) Ferbinteanu, M.; Miyasaka, H.; Wernsdorfer, W.; Nakata, K.; Sugiura, K.; Yamashita, M.; Coulton, C.; Clérac, R. *J. Am. Chem. Soc.* **2005**, *127*, 3090. (d) Wang, S.; Zuo, J.-L.; Gao, S.; Song, Y.; Zhou, H.-C.; Zhang, Y.-Z.; You, X.-Z. *J. Am. Chem. Soc.* **2004**, *126*, 8900.

Chart 1

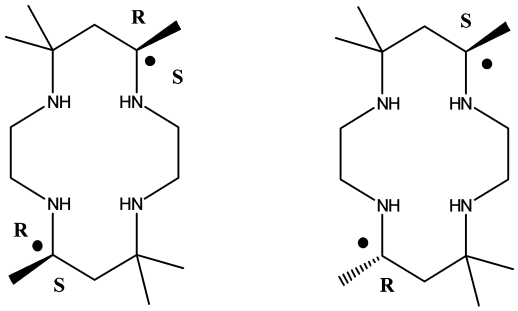

molecules with diverse geometry (squares, extended squares, trigonal bpyramidal, extended trigonal bpyramidal, etc.) and a high-spin ground state.[12e,16c,d,18] Bearing this in mind, we have decided to use cyanometalate complexes to connect the highly thermodynamically stable $[M(rac\text{-CTH})]^{n+}$ complexes (*rac*-CTH = *rac*-5,7,7,12,14,14-hexamethyl-1,4,8,11-tetrazacyclotetradecane), which can adopt the cis-folded configuration (Chart 1).

In principle, the assembly of the cis-folded $[M(rac\text{-CTH})]^{2+}$ cation and the hexacyanometalate anion might lead to cyanide-bridged molecular squares containing terminal cyanide groups, which might further connect either cis-folded or trans-planar $[ML_x]^{n+}$ units, increasing the dimensionality and giving rise to novel magnetic systems. These molecular square-based cyano-bridged systems might eventually exhibit SMM or SCM behavior. The successful isolation of a 1D cyano-bridged Ni_3Fe_2 system constructed from bimetallic squares has proven the validity of this strategy.[19] It should be noted that cyano-bridged metallamacrocycle-containing systems, prepared by controlled self-assembly reactions, are relatively scarce,[16b,g,18−21] and only a dodecanuclear wheel and a few molecular squares or extended molecular squares with paramagnetic metal ions in their structure have been reported to date.[16b,18,19,20a−e,21] We present here the magneto−structural results for two molecular squares (*meso*-CTH-H_2)-$[\{Ni(rac\text{-CTH})\}_2\{Fe(CN)_6\}_2]\cdot 5H_2O$ (**2**) and $[\{Ni(rac\text{-CTH})\}_2\{Fe(CN)_2(bpy)_2\}_2](ClO_4)_4\cdot H_2O$ (**5**), the bimetallic chain $[\{Ni(rac\text{-CTH})\}_2\{Cr(CN)_6\}_2Ni(meso\text{-CTH})]\cdot 4H_2O$ (**3**), the trimetallic chain $[\{Ni(rac\text{-CTH})\}_2\{Fe(CN)_6\}_2Cu(cyclam)]\cdot 6H_2O$ (**4**), the linear pentanuclear complexes $[\{Cu(rac\text{-CTH})\}_3\{Fe(CN)_6\}_2]\cdot 2H_2O$ (**6**) and $[\{Cu(rac\text{-CTH})\}_3\{Cr(CN)_6\}_2]\cdot 2H_2O$ (**7**), and the dinuclear complex $[Cr(rac\text{-CTH})(H_2O)Fe(CN)_6]\cdot 2H_2O$ (**8**).

Experimental Section

Materials. The ligands *rac*- and *meso*-CTH were prepared according to published methods.[22] The complexes $[Ni(rac\text{-CTH})](ClO_4)_2$, $[Ni(meso\text{-CTH})](ClO_4)_2$, $[CrCl_2(rac\text{-CTH})]Cl$, $[Cu(rac\text{-CTH})](ClO_4)_2$, and $[Cu(cyclam](ClO_4)_2$ were prepared according to experimental methods already described.[22−24] $[Fe^{III}(CN)_2(bpy)_2](NO_3)$ and $(Et_4N)_3[Fe(CN)_6]$ were synthesized according to refs 25 and 26, respectively. All other reagents were purchased from commercial sources and used as received.

(*meso*-CTH-H_2)$[\{Ni(rac\text{-CTH})\}_2\{Fe(CN)_6\}_2]\cdot 5H_2O$ (2). A solution of $K_3[Fe(CN)_6]$ (0.03 g, 0.09 mmol) in methanol−water (1:1, 20 mL) was slowly added to a solution of $[Ni(rac\text{-CTH})](ClO_4)_2$ (0.05 g, 0.09 mmol) in the same mixture of solvents (20 mL) with continuous stirring (the color of the solution changed from yellow to brown). The solution was stirred for 5 min before solid (*meso*-CTH-H_2)Cl_2 (0.014 g, 0.038 mmol) was added. The resulting orange solution kept at room temperature for 2 days provided well-developed brown crystals, which were filtered off and air-dried; yield 17%. IR (KBr pellets): ν_{CN} = 2113, 2158 cm^{-1}. Anal. Calcd for $C_{60}H_{120}N_{24}Ni_2Fe_2O_5$: C, 48.47; H, 8.13; N, 22.61. Found: C, 48.52; H, 8.02; N, 22.23.

$[\{Ni(rac\text{-CTH})\}_2\{Cr(CN)_6)\}_2Ni(meso\text{-CTH})]\cdot 4H_2O$ (3). X-ray-quality crystals of this compound were grown in a methanol−water (1:1) mixture by slow diffusion in a H-tube of a solution containing $[Ni(rac\text{-CTH})](ClO_4)_2$ (0.05 g, 0.09 mmol) and $[Ni(meso\text{-CTH})](ClO_4)_2$ (0.025 g, 0.045 mmol) at one arm and a solution of $K_3[Cr(CN)_6]$ (0.03 g, 0.09 mmol) at the other one. After 1−2 weeks on standing at room-temperature, pink crystals of **3** formed. Yield: 5%. IR (KBr pellets): ν_{CN} = 2131, 2151 cm^{-1}. Anal. Calcd for $C_{60}H_{116}N_{24}Ni_3Cr_2O_4$: C, 47.48; H, 7.70; N, 22.15. Found: C, 47.24; H, 7.56; N, 22.05.

$[\{Ni(rac\text{-CTH})\}_2\{Fe(CN)_6\}_2Cu(cyclam)]\cdot 6H_2O$ (4). A solution of tetraethylamonium ferricyanide (0.055 g, 0.18 mmol) in a water−methanol−acetonitrile mixture (2:1:1, 20 mL) was added with continuous stirring to a solution of $[Ni(rac\text{-CTH})](ClO_4)_2$ (0.100 g, 0.18 mmol) in the same mixture of solvents (20 mL). After the resulting brown solution was stirred for 15 min, solid $[Cu(cyclam)](ClO_4)_2$ (0.042 g, 0.09 mmol) was added. The resulting mixture was stirred for 20 min and then filtered. The solution was left standing at room temperature for 2 days, and then crystals of **4**

(18) (a) Berlinguette, C. P.; Galán-Mascarós, J. R.; Dunbar, K. R. *Inorg. Chem.* **2003**, *42*, 3416. (b) Toma, L. M.; Lescouëzec, R.; Cangussu, D.; Llusar, R.; Mata, J.; Spey, S.; Thomas, J. A.; Lloret, F.; Julve, M. *Inorg. Chem. Commun.* **2005**, *8*, 382. (c) Oshio, H.; Tamada, O.; Onodera, H.; Ito, T.; Ikoma, T.; Tero-Kubota, S. *Inorg. Chem.* **1999**, *38*, 5686. (d) Berlinguette, C. P.; Dunbar, K. R. *Chem. Commun.* **2005**, *19*, 2451. (e) Oshio, H.; Yamamoto, M.; Ito, T. *Inorg. Chem.* **2002**, *41*, 5817. (f) Li, D.; Parkin, S.; Wang, G.; Yee, G. T.; Holmes, S. M. *Inorg. Chem.* **2006**, *45*, 2773. (g) Oshio, H.; Onodera, H.; Ito, T. *Chem.*—Eur. J. **2003**, *9*, 3946. (h) Oshio, H.; Onodera, H.; Tamada, O.: Mizutani, H.; Hikichi, T.; Ito, T. *Chem.*—Eur. J. **2000**, *6*, 2523. (i) Nihei, M.; Ui, M.; Yokota, M.; Han, L.; Maeda, A.; Kishida, H.; Okamoto, H.; Oshio, H. *Angew. Chem., Int. Ed.* **2005**, *44*, 6484.

(19) Colacio, E.; Domínguez-Vera, J. M.; Lloret, F.; Rodríguez, A.; Stoeckli-Evans, H. *Inorg. Chem.* **2003**, *42*, 6962.

(20) See for example: (a) Kou, H.-Z.; Gao, S.; Li, C.-H.; Liao, D.-Z.; Wang, R.-J.; Li, Y. *Inorg. Chem.* **2002**, *41*, 4756. (b) Kim, J.; Han, S.; Pokhodnya, K. I.; Migliori, J. M.; Miller, J. S. *Inorg. Chem.* **2005**, *44*, 6983. (c) Li, D.; Zheng, L.; Tang, W. *J. Chem. Soc., Dalton Trans.* **2002**, *14*, 2805. (d) Muga, I.; Gutiérrez-Zorrilla, J. M.; Vitoria, P.; Román, P.; Lloret, F. *Polyhedron* **2002**, *21*, 2631. (e) Jiang, L.; Teng, X.-L.; Lu, T.-B.; Gao, S. *Inorg. Chem.* **2006**, 45, 5018. (f) Falvello, L. R.; Tomás, M. *Chem. Commun.* **1999**, *3*, 273. (g) Klausmeyer, K. K.; Rauchfuss, T. B.; Wilson, S. R. *Angew. Chem., Int. Ed.* **1998**, *37*, 1694. (h) Darensbourg, D. J.; Lee, W.; Adams, M. J.; Yarbrough, J. C. *Eur. J. Inorg. Chem.* **2001**, *11*, 2811. (i) Forniés, J.; Gómez, J.; Lalinde, E.; Moreno, M. T. *Chem.*—Eur. J. **2004**, *10*, 888 and references therein. (j) Kalb, W. C.; Demidowicz, Z.; Speckman, D. M.; Knobler, C.; Teller, R. G.; Hawthorne, M. F. *Inorg. Chem.* **1982**, *21*, 4027. (k) Dawes, H. M.; Hursthouse, M. B.; del Paggio, A. A.; Muetterties, E. L.; Parkins, A. W. *Polyhedron* **1985**, *4*, 379. (l) Olbrich, F.; Kopf, J.; Weiss, E. *J. Organomet. Chem.* **1993**, *456*, 293. (m) Contakes, S. M.; Rauchfuss, T. B. *Angew. Chem., Int. Ed.* **2000**, *39*, 1984. (n) Berlinguette, C. P.; Smith, J. A.; Galán-Mascarós, J. R.; Dunbar, K. R. *C. R. Chim.* **2002**, *5*, 665.

(21) Rebilly, J.-N.; Catala, L.; Charron, G.; Rogez, G.; Rivière, E.; Guillot, R.; Thuéry, P.; Barra, A.-L.; Mallah, T. *Dalton Trans.* **2006**, 2818.

(22) Tait, M. A.; Bush, D. H. *Inorg. Synth.* **1978**, *18*, 10.

(23) Curtis, N. F. *J. Chem. Soc.* **1964**, 2644.

(24) House, D. A.; Hay, R. W.; Ali, M. A. *Inorg. Chim. Acta* **1983**, *72*, 239.

(25) Schilt, A. A. *Anal. Chem.* **1958**, *30*, 1409.

(26) Mascharak, P. K. *Inorg. Chem.* **1986**, *25*, 245.

Table 1. Crystallographic Structure Refinement Data for the Complexes

param	**2**	**3**	**4**	**5**	**6**	**8**
formula	$C_{60}H_{120}N_{24}O_5Fe_2Ni_2$	$C_{60}H_{116}N_{24}O_4Cr_2Ni_3$	$C_{54}H_{108}N_{24}O_6CuFe_2Ni_2$	$C_{76}H_{106}N_{20}O_{17}Cl_4Fe_2Ni_2$	$C_{60}H_{112}N_{24}O_2Fe_2Cu_3$	$C_{22}H_{42}N_{10}O_3FeCr$
M_r	1486.92	1517.90	1482.30	1942.73	1504.06	602.51
cryst system	monoclinic	triclinic	monoclinic	monoclinic	monoclinic	monoclinic
Space group	$P2_1/n$ (No. 14)	$P\bar{1}$ (No. 2)	$C2/c$ (No. 15)	$P2_1/n$ (No. 14)	$C2/c$ (No.. 15)	$P2_1/n$ (No. 14)
a (Å)	*15.5680(9)*	*14.3480(8)*	*25.461(5)*	*17.2075(3)*	*32.841(4)*	*8.8834(10)*
b (Å)	16.6502(12)	*15.0301(8)*	*14.160(3)*	*12.4775(2)*	*16.888(2)*	*19.1585(13)*
c (Å)	16.9719(9)	21.5086(11)	22.410(5)	21.4744(4)	15.647(2)	17.3895(19)
α (deg)	90	77.5615(11)	90	90	90	90
β (deg)	115.530(3)	83.7558(12)	110.385(3)	96.9634(7)	98.237(2)	101.047(4)
γ (deg)	90	64.1686(10)	*90*	*90*	*90*	*90*
V (Å)	*3969.7(4)*	*4076.3(4)*	*7573(3)*	*4576.69(14)*	*8588.7(2)*	*2904.7(5)*
Z	*2*	*2*	*4*	*2*	*4*	*4*
T (K)	173(2)	293(2)	173(2)	173(2)	123(2)	173(2)
λ (Å)	0.710 73	0.710 73	0.710 73	0.710 73	0.710 73	0.710 73
ρ (g cm^{-3})	1.244	1.237	1.300	1.410	1.163	1.378
μ (cm^{-1})	8.83	9.93	11.96	9.05	11.09	9.15
goodness-of-fit	*1.067*	*0.963*	*1.004*	*1.012*	*1.105*	*0.944*
$R1^a$ [$I > 2\sigma(I)$]	*0.0858*	*0.1122*	*0.056*	*0.0542*	*0.0736*	*0.0793*
$wR2^b$ [$I > 2\sigma(I)$]	0.2090	0.2634	0.1406	0.1241	0.1943	0.1305

[a] $R1 = \sum||F_o| - |F_c||/\sum|F_o|$. [b] $wR2 = \{\sum[w(F_o^2 - F_c^2)^2]/\sum[w(F_o^2)^2]\}^{1/2}$.

and [{Cu(cyclam)}$_3${Fe(CN)$_6$}$_2$]·5H$_2$O formed, which were filtered off and air-dried. The red crystals of **4** and the brown crystals of [{Cu(cyclam)}$_3${Fe(CN)$_6$}$_2$]·5H$_2$O were then separated manually. Yield for **4**: 3%. IR (KBr pellets): ν_{CN} = 2153, 2143, 2110 cm^{-1}. Anal. Calcd for **4**, $C_{54}H_{108}N_{24}Ni_2Fe_2CuO_6$: C, 43.97; H, 7.38; N, 22.80. Found: C, 43.89; H, 7.18; N, 22.26.

[{Ni(*rac*-CTH)}$_2${Fe(CN)$_2$(bpy)$_2$}$_2$](ClO$_4$)$_4$·H$_2$O (5). A red solution of [Fe^{III}(bpy)$_2$(CN)$_2$](NO$_3$) (0.043 g, 0.17 mmol) in methanol−water (1:1, 20 mL) was added to a yellow solution of [Ni(*rac*-CTH)](ClO$_4$)$_2$ (0.094 g, 0.17 mmol) in the same mixture of solvents (20 mL). The red solution was filtered and left on standing for 2 days at room temperature, whereupon red crystals of **5** formed, which were filtered off and air-dried. Yield: 34%. IR (KBr pellets): ν_{CN} = 2105, 2123 cm^{-1}. Anal. Calcd for $C_{76}H_{106}N_{20}Ni_2Fe_2Cl_4O_{17}$: C, 46.99; H, 5.50; N, 14.42. Found: C, 46.81; H, 5.24; N, 14.10.

[{Cu(*rac*-CTH)}$_3${Fe(CN)$_6$}$_2$]·2H$_2$O (6). The reaction of a blue solution of [Cu(*rac*-CTH)](ClO$_4$)$_2$ (0.30 g, 0.55 mmol) in methanol−water (1:1, 20 mL) and an orange solution of K$_3$[Fe(CN)$_6$] (0.18 g, 0.55 mmol) in the same mixture of solvents (15 mL) lead to a green solution, which kept at room temperature for several days afforded green crystals of **6**, which were filtered off and air-dried. Yield: ca. 37%. IR (KBr pellets): ν_{CN} 2118, 2155 cm^{-1}. Anal. Calcd for $C_{60}H_{112}N_{24}Cu_3Fe_2O_2$: C, 47.92; H, 7.51; N, 22.35. Found: C, 47.69; H, 7.26; N, 22.14.

[{Cu(*rac*-CTH)}$_3${Cr(CN)$_6$)} $_2$]·2H$_2$O (7). Compound **7** was prepared by the same procedure as for **6** but using K$_3$[Cr(CN)$_6$] instead of K$_3$[Fe(CN)$_6$]. The resulting blue solution was left standing for 2 days at room temperature, and then blue crystals formed, which were filtered off and air-dried. Yield: 10%. IR (KBr pellets): ν_{CN} 2131, 2151 cm^{-1}. Anal. Calcd for $C_{60}H_{112}N_{24}Cu_3Cr_2O_2$: C, 49.04; H, 7.68; N, 22.88. Found: C, 48.63; H, 7.39; N, 22.45.

[Cr(*rac*-CTH)(H$_2$O)Fe(CN)$_6$]·2H$_2$O (8). To a solution of [CrCl$_2$(*rac*-CTH)]]Cl (0.05 g, 0.11 mmol) in methanol−water (1:1, 10 mL) was added with continuous stirring a solution of K$_3$[Fe(CN)$_6$] (0.037 g, 0.11 mmol) in the minimum amount of the same mixture of solvents, and the color of the solution changed from green to brown. This solution was placed at one arm of a H-tube, and a solution of [Cu(cyclam)](ClO$_4$)$_2$ (0.06 g, 0.11 mmol) was placed at the other arm. Red crystals of **8** were formed on standing at room temperature for 2 weeks. Yield: 8%. Anal. IR (KBr pellets): ν_{CN} 2103, 2149 cm^{-1}. Calcd for $C_{22}H_{42}N_{10}CrFeO_3$: C, 43.86; H, 7.03; N, 23.25. Found: C, 44.06; H, 6.91; N, 23.51.

Physical Characterization. Elemental analyses were carried out at the Instrumentation Scientific Centre of the University of Granada on a Fisons-Carlo Erba analyzer model EA 1108. The analysis of metals was performed by SEM on a LEO, model GEMINI-1530 microscope at the Instrumentation Scientific Centre of the University of Granada. IR spectra were recorded on a The IR spectra on powdered samples were recorded with a ThermoNicolet IR200FTIR by using KBr pellets. Magnetization and variable-temperature (1.9−300 K) magnetic susceptibility measurements on polycrystalline samples were carried out with a Quantum Design SQUID operating at different magnetic fields. Magnetization versus applied field measurements were carried out at 2.0 K in the field range 0−5 T. Alternating current susceptibility measurements were performed in the frequency range 10−100 Hz and under an oscillating magnetic field of 1 Oe. The experimental susceptibilities were corrected for the diamagnetism of the constituent atoms by using Pascal's tables.[27]

X-ray Crystallography. Single-crystal data for **2** and **5** were measured on a Enraf Nonius KappaCCD diffractometer; complex **6** was measured on a Bruker Smart 1000, whereas those for the rest of the compounds were collected on a Bruker Smart Apex CCD diffractometer, using graphite-monochromatized Mo Kα radiation. All data sets were corrected for Lorentz and polarization effects. A summary of the crystallographic data and structure refinements is given in Table 1.

The structures were solved by direct methods and refined on F^2 by the program SHELXL97[28] or SHELXTL.[29]

For **2**, the asymmetric unit of the structure consists of half of [*meso*-CTH-H$_2$]$^{2+}$ cation and half of [{Ni(*rac*-CTH)}$_2${Fe(CN)$_6$}$_2$]$^{2-}$ anion and 2.5 disordered crystal water molecules. The NH$_2$ group of the cation was positioned at N11 on the basis of the H-bond system and R values. Non-hydrogen atoms, except the disordered oxygen atoms, were refined with anisotropic thermal displacement parameters. The hydrogen atoms of the macrocyclic ligands, expect

(27) Khan, O. *Molecular Magnetism*; VCH Publishers, Inc.: Weinheim, Germany, 1993.
(28) Sheldrick, G. M. *SHELX97*; University of Göttingen: Göttingen, Germany, 1997.
(29) Sheldrick, G. M. *SHELXTL*, version 6.12; Bruker AXS: Madison, WI, 2001.

the hydrogen at N12, were treated as riding atoms using the SHELX97 default parameters. Hydrogen atoms of the water molecules could not be reliably positioned.

For **3**, asymmetric unit of the structure consists of two halves of two $[Ni(rac\text{-}CTH)]_2[Cr(CN)_6]_2^{2-}$ bimetallic units, two halves of two trans-planar $[Ni(meso\text{-}CTH)]^{2+}$ units, and four crystal water molecules with two of the water molecules being disordered. One of the trans planar units is not well defined, and several DFIX restraints were utilized to obtain reasonable bond parameters for the unit. Moreover, refinement of site occupation parameters of the disordered oxygen atoms did not converge well and the parameters were fixed to 0.5. Owing to the modest quality of the data, only metal atoms were refined with anisotropic thermal displacement parameters, and the rest of the non-hydrogen atoms were refined with isotropic thermal displacement parameters. The hydrogen atoms of the macrocyclic ligands were treated as riding atoms using the SHELX97 default parameters. Hydrogen atoms of the water molecules could not be reliably positioned.

For **4**, the asymmetric unit of the structure consists of half of $[\{Ni(rac\text{-}CTH)\}_2\{Fe(CN)_6\}_2]^{2-}$ anion, half of $[Cu(cyclam)]^{2+}$ cation and three disordered water molecules. As reliable refinement of site occupation parameters of oxygen atoms failed, a parameter of 0.5 was fixed for each oxygen position. Non-hydrogen atoms, except the disordered oxygen atoms, were refined with anisotropic thermal displacement parameters. The hydrogen atoms of the macrocyclic ligands were treated as riding atoms using the SHELX97 default parameters. Hydrogen atoms of the water molecules could not be reliably positioned.

For **5**, the asymmetric unit of the structure consists of half of $[\{Fe(CN)_2(bpy)_2\}_2\{Ni(rac\text{-}CTH)\}_2]^{4+}$ cation and two disordered ClO_4^- anions. For both anions, each atom occupies two positions and the anions were refined as rigid groups. Non-hydrogen atoms, except the disordered oxygen atoms, were refined with anisotropic thermal displacement parameters. The hydrogen atoms of the bpy and macrocyclic ligands were treated as riding atoms using the SHELX97 default parameters.

The crystal quality for complex **6** was not good, and the peaks were broad. The structure was solved in *C*2/*c*, and the molecule lies on a 2-fold axis which passes through C33 and C31 of the central macrocycle. Hence, the asymmetric unit contains 1.5 $\{[Cu(rac\text{-}CTH)]^{2+}$ cations and one $[Fe(CN)_6]^{3-}$ anion, with one water of crystallization. The central macrocycle is also disordered, and the copper ion (Cu2) was modeled with 50% occupancy of two related sites. The disorder was not reduced on refinement in the lower symmetry group *Cc*. Both macrocycles show disorder of the methyl groups. All the non-hydrogen atoms were refined using anisotropic atomic displacement parameters, and hydrogen atoms were inserted at calculated positions using a riding model except for those on the water solvate molecules, the disordered tertiary carbons, or the amines of the disordered macrocycle; these were not located or included in the model.

For **8**, the asymmetric unit of the structure consists of a $[Cr(rac\text{-}CTH)(H_2O)Fe(CN)_6\}]$ complex unit and two noncoordinated water molecules. Non-hydrogen atoms were refined with anisotropic thermal displacement parameters. The hydrogen atoms of the *rac*-CTH ligand were treated as riding atoms using the SHELX97 default parameters, while the hydrogen atoms, except two, of the water molecules were picked from a difference Fourier map and refined with fixed O−H distance.

Computational Details. All theoretical calculations were carried out with the hybrid B3LYP method,[30−32] as implemented in the GAUSSIAN03 program.[33] Double-ζ quality basis sets proposed by Ahlrichs and co-workers have been used for all atoms, except for the metal atoms where we have used a triple-ζ basis.[34,35] The broken symmetry approach has been employed to describe the unrestricted solutions of the antiferromagnetic spin states.[36−39] The geometries of the studied models for the mononuclear complexes were built from the experimental crystal structures. A quadratic convergence method was used to determine the more stable wave function in the SCF process.[40] This determination is not a simple task for this type of systems due to the fact that several different solutions very close in energy can be found. In our case, these solutions correspond roughly to the same configuration and only slight changes are revealed.[41−44] However, the energy of these solutions vary by a hundred or even a thousand cm^{-1}.[41−44] To avoid this problem the stability test was carried out on the single-determinant wave function of the more stable solution.[45,46] Additional calculations have been done in a polarizable continuum model (PCM) where the cavity is created via a series of overlapping spheres.[47,48] The atomic spin densities were obtained from natural bond orbital (NBO) analysis.[49−51]

(30) Becke, A. D. *Phys. Rev. A* **1988**, *38*, 3098.
(31) Lee, C.; Yang, W.; Parr, R. G. *Phys. Rev. B* **1988**, *37*, 785.
(32) Becke, A. D. *J. Chem. Phys.* **1993**, *98*, 5648.
(33) Frisch, M. J.; Trucks, G. W.; Schlegel, H. B.; Scuseria, G. E.; Robb, M. A.; Cheeseman, J. R.; Montgomery, J.; Vreven, J. A., T.; Kudin, K. N.; Burant, J. C.; Millam, J. M.; Iyengar, S. S.; Tomasi, J.; Barone, V.; Mennucci, B.; Cossi, M.; Scalmani, G.; Rega, N.; Petersson, G. A.; Nakatsuji, H.; Hada, M. Ehara, M.; Toyota, K.; Fukuda, R.; Hasegawa, J.; Ishida, M.; Nakajima, T.; Honda, Y.; Kitao, O.; Nakai, H.; Klene, M.; Li, X.; Knox, J. E.; Hratchian, H. P.; Cross, J. B.; Bakken, V.; Adamo, C.; Jaramillo, J.; Gomperts, R.; Stratmann, R. E.; Yazyev, O.; Austin, A. J.; Cammi, R.; Pomelli, C.; Ochterski, J. W.; Ayala, P. Y.; Morokuma, K.; Voth, G. A.; Salvador, P.; Dannenberg, J. J.; Zakrzewski, V. G.; Dapprich, S.; Daniels, A. D.; Strain, M. C.; Farkas, O.; Malick, D. K.; Rabuck, A. D.; Raghavachari, K.; Foresman, J. B.; Ortiz, J. V.; Cui, Q.; Baboul, A. G.; Clifford, S.; Cioslowski, J.; Stefanov, B. B.; Liu, G.; Liashenko, A.; Piskorz, P.; Komaromi, I.; Martin, R. L.; Fox, D. J.; Keith, T.; Al-Laham, M. A.; Peng, A. C.; Nanayakkara, Y.; Challacombe, M.; Gill, P. M. W.; Johnson, B.; Chen, W.; Wong, M. W.; Gonzalez, C.; Pople, J. A. In *Gaussian 03*, revision C.02, and *Gaussian 03*, revision C.02 ed.; Gaussian, Inc.: Wallingford, CT, 2004.
(34) Schaefer, A.; Horn, A.; Ahlrichs, R. *J. Chem. Phys.* **1992**, *97*, 2571.
(35) Schaefer, A.; Huber, C.; Ahlrichs, R. *J. Chem. Phys.* **1994**, *100*, 5829.
(36) Ruiz, E.; Cano, J.; Alvarez, S.; Alemany, P. *J. Comput. Chem.* **1999**, *20*, 1391.
(37) Ruiz, E.; Rodríguez-Fortea, A.; Cano, J.; Alvarez, S.; Alemany, P. *J. Comput. Chem.* **2003**, *24*, 982.
(38) Ruiz, E.; Alvarez, S.; Cano, J.; Polo, V. *J. Chem. Phys.* **2005**, *123*, 164110/1.
(39) Rajaraman, G.; Ruiz, E.; Cano, J.; Alvarez, S. *Chem. Phys. Lett.* **2005**, *415*, 6.
(40) Bacskay, G. B. *Chem. Phys.* **1981**, *61*, 385404.
(41) Toma, L. M.; Delgado, F. S.; Ruiz-Perez, C.; Carrasco, R.; Cano, J.; Lloret, F.; Julve, M. *Dalton Trans.* **2004**, 2836.
(42) Toma, L.; Lescouezec, R.; Vaissermann, J.; Delgado, F. S.; Ruiz-Perez, C.; Carrasco, R.; Cano, J.; Lloret, F.; Julve, M. *Chem.*—Eur. J. **2004**, *10*, 6130.
(43) Toma, L.; Toma, L. M.; Lescouezec, R.; Armentano, D.; De Munno, G.; Andruh, M.; Cano, J.; Lloret, F.; Julve, M. *Dalton Trans.* **2005**, 1357.
(44) Toma, L.; Lescouezec, R.; Pasán, J.; Ruiz-Perez, C.; Vaissermann, J.; Cano, J.; Carrasco, R.; Wernsdorfer, W.; Lloret, F.; Julve, M. *J. Am. Chem. Soc.* **2006**, in press.
(45) Seeger, R.; Pople, J. A. *J. Chem. Phys.* **1977**, *66*, 3045.
(46) Bauernschmitt, R.; Ahlrichs, R. *J. Chem. Phys.* **1996**, *104*, 9047.
(47) Tomasi, J.; Mennucci, B.; Cancès, E. *J. Mol. Struct. (THEOCHEM)* **1999**, *464*, 211 and references therein.
(48) Cossi, M.; Rega, N.; Scalmani, G.; Barone, V. *J. Comput. Chem.* **2003**, *24*, 669 and references therein.
(49) Carpenter, J. E.; Weinhold, F. *J. Mol. Struct.* **1988**, *46*, 41.
(50) Reed, A. E.; Curtis, L. A.; Weinhold, F. *Chem. Rev.* **1988**, *88*, 899.
(51) Weinhold, F.; Carpenter, J. E. *The Structure of Small Molecules and Ions*; Plenum: New York, 1988; p 227.

Results and Discussion

The assembly of $[Fe(CN)_6]^{3-}$ and $[Ni(rac\text{-}CTH)]^{2+}$ building blocks yielded the complex $[\{Ni(rac\text{-}CTH)\}_3\{Fe(CN)_6\}_2]\cdot 4H_2O$ (**1**), which was previously reported by us[20] and is made of chains of molecular squares. We think that the mechanism of this reaction might be as follows: in a first step the folded cis configuration of the $[Ni(rac\text{-}CTH)]^{2+}$ would lead to distorted bimetallic molecular squares Fe_2Ni_2 containing terminal cyanide groups, which, in a second step, would connect these molecular squares to disordered trans-planar $[Ni(rac\text{-}CTH)]^{2+}$ units (*RR* and *SS* enantiomers are coordinated to Ni ion), leading ultimately to the chain. If this is so, in principle, it should be possible to isolate discrete molecular squares from the 1:1 reaction between $[M(CN)_6]^{3-}$ and $[Ni(rac\text{-}CTH)]^{2+}$. All attempts to obtain discrete molecular squares by assembling these building blocks in the presence of bulky isolating cations, such as PPh_4^+ and NBu_4^+, were unsuccessful. However, the use of the diprotonated *meso*-CTH-H_2^{2+} itself as a cation allowed the isolation of the discrete distorted molecular square $(meso\text{-}CTH\text{-}H_2)[\{Ni(rac\text{-}CTH)\}_2\{Fe(CN)_6\}_2]\cdot 5H_2O$ (**2**). The presence of discrete molecular squares as intermediates in the formation of the chain complexes **1** and **2** opened the door toward the synthesis of ligand mixed bimetallic and trimetallic chains. Thus, the reaction of $[Ni(rac\text{-}CTH)]^{2+}$ and $[Fe(CN)_6]^{3-}$ in 1:1 stoichiometric ratio and the further reaction with either $[Ni(meso\text{-}CTH)]^{2+}$ or $[Cu(cyclam)]^{2+}$ building blocks afforded in low yield the bimetallic chain $[\{Ni(rac\text{-}CTH)\}_2\{Cr(CN)_6\}_2Ni(meso\text{-}CTH)]\cdot 4H_2O$ (**3**) and the heterotrimetallic chain compound $[\{Ni(rac\text{-}CTH)\}_2\{Fe(CN)_6\}_2Cu(cyclam)]\cdot 6H_2O$ (**4**), respectively. It should be noted that, in the latter case, the major product was not **4** but the 1D complex $[\{Cu(cyclam\}_3\{Fe(CN)_6\}_2]\cdot 5H_2O$.

An alternative route to discrete bimetallic molecular squares is that of using a *cis*-cyanometalate building block having four coordination positions blocked by end-cap ligands. Thus, the reaction between $[Fe^{III}(CN)_2(bpy)_2]^+$ and $[Ni(rac\text{-}CTH)]^{2+}$ building blocks afforded the compound $[\{Ni(rac\text{-}CTH)\}_2\{Fe(CN)_2(bpy)_2\}_2](ClO_4)_4\cdot H_2O$ (**5**). In the course of the reaction the Fe^{III} of $[Fe^{III}(CN)_2(bpy)_2]^+$ was reduced to the Fe^{II} ion. When $[Cu(rac\text{-}CTH)]^{2+}$ was used instead of $[Ni(rac\text{-}CTH)]^{2+}$, the expected molecular square did not form but pentanuclear molecules $[\{Cu(rac\text{-}CTH)\}_3\{Fe(CN)_6\}_2]\cdot 2H_2O$ (**6**) and $[\{Cu(rac\text{-}CTH)\}_3\{Cr(CN)_6\}_2]\cdot 2H_2O$ (**7**) were obtained instead. In these two latter compounds the plasticity of the copper(II) coordination sphere and the Jahn−Teller distortion are the main factors preventing the formation of cyclic structures. Finally, the reaction between $[CrCl_2(rac\text{-}CTH)]^+$ and $[Fe(CN)_6]^{3-}$ led to the binuclear complex $[Cr(rac\text{-}CTH)(H_2O)Fe(CN)_6]\cdot 2H_2O$ (**8**). In this case, the coordination of a water molecule to the Cr(III) ion avoids the propagation of the structure.

Description of the Structures. (*meso*-CTH-H_2)[{Ni(*rac*-CTH)}$_2${Fe(CN)$_6$}$_2$]·5H_2O (2). The structure consists of distorted cyanide-bridged centrosymmetric $[\{Ni(rac\text{-}CTH)\}_2\{Fe(CN)_6\}_2]^{2-}$ squares, *meso*-CTH-H_2^{2+} cations, and disordered water molecules of crystallization (Figure 1).

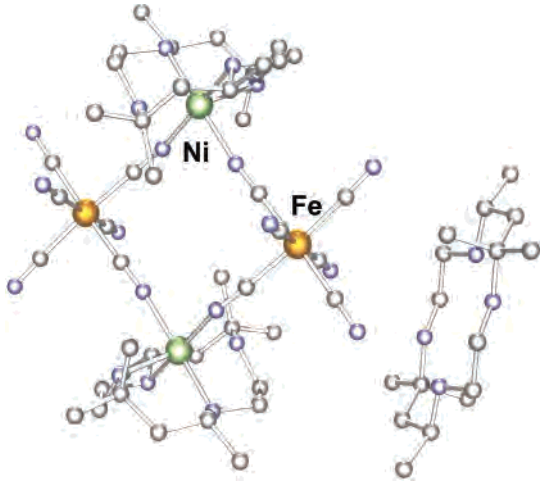

Figure 1. Perspective drawing of the structure of **2**: Fe^{III} (orange); Ni^{II} (green); N (blue); carbon (gray). Water molecules are omitted.

Within the squares, Ni^{II} and Fe^{III} atoms at the corners are alternatively bridged by cyanide groups that are located at the edges. The Fe···Ni distances are 5.0244(13) and 5.0886(11) Å, whereas the Ni···Ni and Fe···Fe distances along the diagonals are 6.979(2) and 7.320(2) Å, respectively. As in **1**, also in **2**, there exists a center of symmetry at the barycenter of the square, and therefore, the four metal atoms are forced to be coplanar with Fe−Ni−Fe and Ni−Fe−Ni angles of 92.73(2) and 87.27(2)°, respectively. In the bridging region, the Fe−C−N bond angles are almost linear (174.8(6) and 176.7(6)°), whereas the Ni−N−C bond angles are significantly bent (154.3(6) and 172.0(6)°). The nickel(II) ions exhibit a NiN_6 distorted octahedral coordination environment, made of four nitrogen atoms from the *rac*-CTH ligand, which adopts a folded conformation, and two cyanide nitrogen atoms situated at cis positions. Bond lengths and angles involving $[Ni(rac\text{-}CTH)]^{2+}$ and $[Fe(CN)_6]^{3-}$ units are similar to those observed in **1**, whereas bond lengths and angles for the *meso*-CTH-H_2^{2+} cation are in agreement with those reported for other *meso*-CTH-H_2^{2+}-containing compounds.[52] Square anions are not well isolated in the structure but linked by hydrogen-bonding interactions involving two NH groups of the coordinated macrocycle, one nitrogen atom of a terminal cyanide ligand belonging to a neighboring square and one disordered water molecule, with N3···N9, N2···O1a, and N2···O1b donor−acceptor distances of 2.993(10), 3.30(2), and 3.17(3) Å, respectively. Terminal cyanide ligands also form medium to weak hydrogen bond interactions with water molecules and two nitrogen atoms belonging to the *meso*-CTH-H_2^{2+} cation with N7···O3, N7···O1b, N10···O2b, N4····N6, and N11−N8 distances of 2.97(2), 2.76(4), 2.88(3), 3.18(7), and 2.825(9) Å, respectively, ultimately leading to a 3D supramolecular network. The shortest interchain metal−metal separation of 6.8793(13) Å is for Ni−Fe. Although some cyanide-bridged Fe^{III}/Ni^{II} bimetallic "extended squares" have been recently reported, such as $[\{Ni(bpy)_2(H_2O)\}\{Ni(bpy)_2\}_2\{Fe(CN)_6\}_2]\cdot 12H_2O$ (bpy =

(52) (a) Gao, E. Q.; Tang, J. K.; Leng, X. B.; Liao, D. Z.; Jiang, Z. H.; Yan, S. P. *Gaodeng Xuexiao Huaxue Xuebao* **2000**, *21*, 663. (b) Suchá, V.; Sivák, M.; Tyrselová, J.; Marek, J. *Polyhedron* **1997**, *16*, 2837.

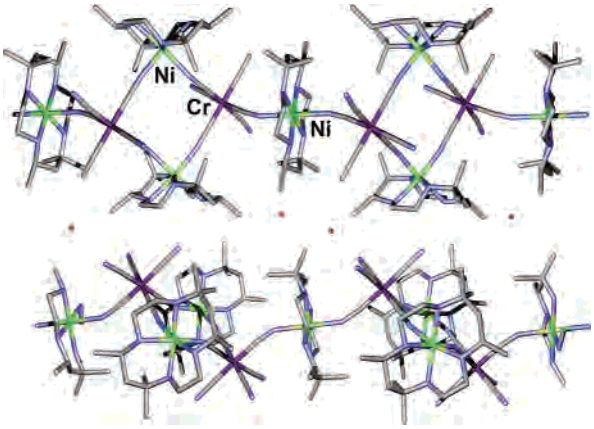

Figure 2. Perspective drawing of the structure of **3**: Cr^{III} (purple); Ni^{II} (green); N (blue); C (gray); O (red).

2,2′-bpyridine)[18a] and $[Fe(Tp)(CN)_3\}_4\{Ni(MeCN)(H_2O)_2\}_2]\cdot 10H_2O$ (Tp = hydrotris(1-pyrazolyl)borate),[20b] as far as we know, only exists one reported example of an isolated cyanide-bridged Fe^{III}/Ni^{II} bimetallic molecular square, $[TpFe(CN)_3Ni(DMF)_4]_2(OTf)_2\cdot 2DMF$ ($OTf = CF_3SO_3^-$).[16b]

$[\{Ni(rac\text{-}CTH)\}_2\{Cr(CN)_6\}\}_2Ni(meso\text{-}CTH)]\cdot 4H_2O$ (3). The structure of **3** (Figure 2) is similar to that of **1** and consists of an alternating arrangement of $[Ni(rac\text{-}CTH)\}_2\{Cr(CN)_6\}_2]$ bimetallic distorted square units and trans-planar $[Ni(meso\text{-}CTH)]^{2+}$ units bridged by cyanide groups to afford 1D chains running along the *b* axis. Water molecules of crystallization, which are located between the chains, contribute to stabilize the structure. In contrast to **1**, there are two similar but crystallographically nonequivalent chains in the structure of **3**.

Within the centrosymmetric Cr_2Ni_2 distorted square units, the four metal ions occupy the corners and four cyanide bridging ligands are located at the edges, with Cr1···Ni1 distances of 5.244(2) and 5.156(2) Å for one type of chain and Cr31···Ni31 distances of 5.186(2) and 5.196(2) Å for the other one. The Cr1···Cr1 and Cr31−Cr31 distances along the diagonals are 7.365(3) and 7.316(3) Å, whereas the Ni1···Ni1 and Ni31···Ni31 distances are 7.343(3) and 7.367(3) Å. These distances are somewhat longer than those observed in **2**, which is due, at least partly, to the fact that the Cr−C distances in the $[Cr(CN)_6]^{3-}$ units of **3** (in the range 1.995(14)−2.068(10) Å) are also longer than the Fe−C distances in the low-spin $[Fe(CN)_6]^{3-}$ units (in the range 1.929(6) Å−1.961(9) Å). In the bridging region of the square units, Cr−C−N bond angles are 173.6(9) and 175.8(9)° for one chain and 178.0(10) and 179.6(10)° for the other one, whereas the Ni−N−C angles are 157.4(8) and 171.2(9) and 159.5(9) and 167.0(9)°, respectively. The metal atoms in the Cr_2Ni_2 square are forced to be coplanar because of the existence of a center of symmetry at the barycenter of each square unit, the Cr1···Ni1···Cr1, Cr31···Ni31···C31, Ni1···Cr1···Ni, and Ni31···Cr31···Ni31angles being 90.17(3) and 89.60(3) and 89.83(3) and 90.40(3)°, for the two chains.

For the two nonequivalent chains, in the square units the $Ni-N_{macro}$ and $Ni-N_{cyanide}$ bond lengths are in the ranges 2.107(10)−2.192(11) and 2.048(10)−2.104(9) Å, respectively, whereas cis and trans angles are in the ranges 81.7(4)−106.9(4) and 166.8(4)−171.1(4)°, respectively. Bond distances and angles around distorted octahedral Ni(II) atoms of the square units are similar to those observed in **2**. Cr ions exhibit a slightly distorted octahedral coordination geometry with Cr−C and C−Cr−C bond distances and angles similar to those observed for other complexes containing $[Cr(CN)_6]^{3-}$ bridging units.[53] Square units are further connected to $[trans\text{-}Ni(meso\text{-}CTH)]^{2+}$ ions through one of the cyanide groups of each $[Cr(CN)_6]^{3-}$ unit to form the chain. A remarkable difference between **3** and **1** is that in the former the cyanide bridging groups of the tridentate $[Cr(CN)_6]^{3-}$ anion exhibit a *fac* disposition, whereas in the latter the cyanide bridging groups of the $[Fe(CN)_6]^{3-}$ anion exhibit a *mer* disposition. A similar extension of the structure by addition of extra ML building blocks to cyanide-bridged $M^{III}M^{II}$ square units has been also observed in **1**, in the pentanuclear clusters $[\{Ni(bpy)_2(H_2O)\}\{Ni(bpy)_2\}_2\{Fe(CN)_6\}_2]$[18a] and $[\{Co(bpy)_2(H_2O)\}\{Co(bpy)_2\}_2\{Co(CN)_6\}_2]$[54] and in the decameric cluster $[\{Zn(phen)_2\{Fe(CN)_6\}_2\{Zn(phen)_2Zn(phen)_2(H_2O)Fe(CN)_6\}_2]$.[20m] In the bridging region between the squares and *trans*-$[Ni(meso\text{-}CTH)]^{2+}$ units of the chains of **3**, the Cr1···Ni2 and Cr31···Ni32 distances are 5.137(2) and 5.154(2) Å, the Cr1−C21−N9 and Cr31−C51−N39 angles are 170.5(9) and 172.2(10)°, and the Ni2−N9−C21 and Ni32−N39−C51 angles are 155.9(9) and 154.7(9)°. The Ni(II) atoms of the *trans*-$[Ni(meso\text{-}CTH)]^{2+}$ units, which are placed at inversion centers, exhibit tetragonally elongated distorted geometries, the longest bond distances involving the nitrogen atoms of the trans cyanide groups, with Ni−N bond distances in the ranges 2.060(12)−2.135(10) and 1.989(17)−2.125(10) Å, respectively. The cis bond angles are in the ranges 84.5(5)−95.5(5) and 84.4(6)−95.6(5)°, respectively, whereas the trans angles are 180° owing to symmetry. The chains running along the *b* axis are not isolated but connected by hydrogen bonds involving one of the terminal cyanide groups of a chain and two NH groups of a folded $[Ni(rac\text{-}CTH)]^{2+}$ unit of the neighboring and crystallographically nonequivalent chain, with N1···N40 and N3···N40 distances of 3.283(15) and 3.209(16) Å, respectively. In addition, the NH groups of the former chain are involved in hydrogen bond interactions with the O1 atom of a solvate water molecule (O1···N31 and O1···N33 distances of 3.089(14) and 3.212(14) Å, respectively). The dihedral angle between distorted Cr_2Ni_2 squares of neighboring nonequivalent chains is 75°, the shortest interchain metal···metal distance being 6.757(2) Å.

$[\{Ni(rac\text{-}CTH)\}_2\{Fe(CN)_6\}\}_2Cu(cyclam)]\cdot 6H_2O$ (4). The structure of **4** is made up of an alternating arrangement of cyanide-bridged centrosymmetric distorted square $[\{Ni(rac\text{-}CTH)\}_2\{Fe(CN)_6\}_2]^{2-}$ anions and *trans*-$[Cu(cyclam)]^{2+}$ cations linked by cyanide groups to form a trimetallic Fe−

(53) (a) Fu, D. G.; Chen, J.; Tan, X. S.; Jiang, L. J.; Zhang, S. W.; Zheng, P. J.; Tang, W. X. *Inorg. Chem.* **1997**, *36*, 220. (b) El Fallah, M. S.; Ribas, J.; Solans, X.; Font-Bardia, M. *J. Chem. Soc., Dalton Trans.* **2001**, *3*, 247. (c) Thétiot, F.; Triki, S.; Sala, J.; Gómez-García, C. J.; Golhen, S. *Chem. Commun.* **2002**, *10*, 1078. (d) Marvilliers, A.; Parsons, S.; Rivière, E.; Audière, J.-P.; Kurmoo, M.; Mallah, T. *Eur. J. Inorg. Chem.* **2001**, *5*, 1287.

(54) Rodríguez, A.; Kivekäs, R.; Sillanpää, R.; Sakiyama, H.; Colacio, E. Manuscript in preparation.

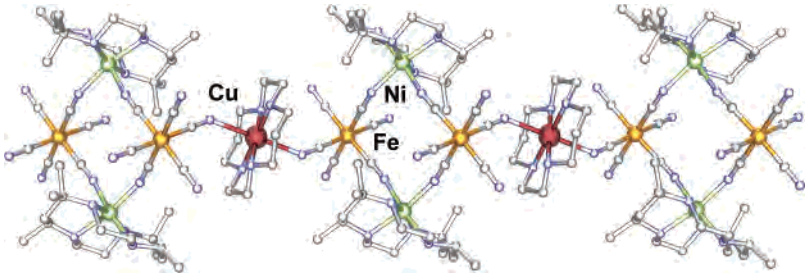

Figure 3. Perspective drawing of the structure of **4**. Fe^{III} (orange); Ni^{II} (green); Cu^{II} (red); N (blue); C (gray). Water molecules have been omitted for clarity.

Ni−Cu zigzag chain running diagonally in *ab* plane and six disordered water molecules of crystallization/formula unit (Figure 3). Bond distances and angles within the molecular squares are similar to those observed in **2**. Thus, the Fe···Ni distances along the edges are 5.290(3) and 5.0009(13) Å, whereas Ni···Ni and Fe···Fe distances along the diagonals are 6.9555(14) and 7.3794(15) Å, respectively. The Fe···Ni···Fe and Ni···Fe···Ni angles are 93.39(1) and 86.61(1)°, whereas, in the bridging region, the Ni−N−C angles are 171.4(3) and 151.3(3)° and the Fe−C−N angles are 174.0(4) and 175.0(3)°. The square Fe_2Ni_2 units are linked to the centrosymmetric trans planar $[Cu(cyclam)]^{2+}$ units through one of the cyanide groups of the tridentate $[Fe(CN)_6]^{3-}$ anions leading to the chain. As in **3**, the cyanide-bridging groups of the tridentate $[Fe(CN)_6]^{3-}$ unit adopt a *fac* disposition around iron(III) ion. The copper(II) ion, which is located on an inversion center, exhibits a tetragonally elongated CuN_6 coordination environment. In this description, the nitrogen atoms of the macrocycle ligands occupy the equatorial positions with Cu−N distances of about 2 Å, whereas the nitrogen atoms belonging to the cyanide bridging ligands occupy the axial positions at a longer distance of 2.460(4) Å as a consequence of the Jahn−Teller effect of the copper(II) atom. In the Fe···Cu bridging region, the Fe−C21−N9 and Cu−N9−C21 angles are 177.6(4) and 136.5(3)°, respectively, with an Fe···Cu distance of 5.1367(12) Å. The dihedral angle between the plane through the Fe_2Ni_2 square and the CuN_4 coordination plane of $[Cu(cyclam)]^{2+}$ cation is 42°. Chains are connected by hydrogen-bonding interactions involving one of the terminal cyanide groups of a chain and one the NH group of the folded $[Ni(rac\text{-CTH})]^{2+}$ unit of the neighboring chain with N7···N1 distance of 3.148(5) Å. In addition, the crystal structure is stabilized by hydrogen bonds involving NH groups of the CTH and cyclam macrocycles, disordered water molecules, and terminal cyanide groups. The shortest metal−metal interchain distance is 6.6992(15) Å.

It is interesting to note that, as far as we know, there exists only one additional example of a heterotrimetallic system containing cyano-bridging ligand between each pair of the metal ions.[18d]

$[\{Ni(rac\text{-CTH})\}_2\{Fe(CN)_2(bpy)_2\}_2](ClO_4)_4\cdot H_2O$ (5). The structure of **5** (Figure 4) is made up of centrosymmetric cationic distorted squares of formula $[\{Ni(rac\text{-CTH})\}_2\{Fe(CN)_2(bpy)_2\}_2]^{4+}$ and disordered water molecules and perchlorate anions.

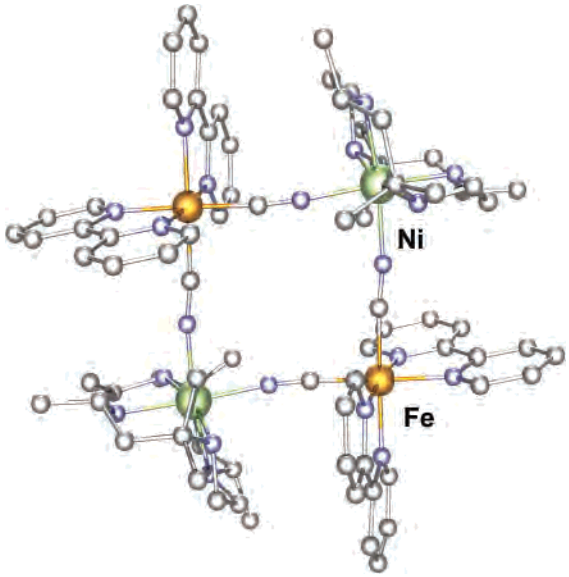

Figure 4. Perspective drawing of the square unit $[\{Ni(rac\text{-CTH})\}_2\{Fe(CN)_2(bpy)_2\}_2]^{4+}$ of **5**: Fe^{III} (orange); Ni^{II} (green); N (blue); C (gray).

Within the molecular square, low-spin Fe^{II} and Ni^{II} ions, placed at the corners, are alternately bridged by cyanide groups. As in compounds **1**−**4**, each Ni(II) ion in **5** exhibits a NiN_6 distorted octahedral coordination environment, made of four nitrogen atoms belonging to the *rac*-CTH ligand and two nitrogen cyanide atoms located at cis positions. Bond distances and angles involving Ni(II) ions are close to those found in compounds **1**−**4**. Each iron(II) ion in **5** exhibits a distorted octahedral FeC_2N_4 coordination environment, which is made of four nitrogen atoms from two bpy ligands and two cis cyanide carbon atoms. Bond distances and angles involving the iron(II) ion are similar to those found in other $Fe^{II}(CN)_2(bpy)_2$-containing compounds.[18g−i,55] The Fe···Ni distances along the edges are 5.0788(8) and 5.0960(7) Å, whereas Ni···Ni and Fe···Fe distances along diagonals are 7.5731(10) and 6.7952(11) Å. The Ni···Fe···Ni and Fe···Ni···Fe angles are 96.20(1) and 83.80(1)°, respectively. As expected for the Fe−C−N-bridges, the Fe−C17−N5 and Fe−C18−N6 angles of 174.5(3) and 173.8(4)° are closer to linearity than the Ni−N5−C17 and Ni−N6−C18 angles of 162.4(3) and 171.0(3)°. This is due to the stronger covalent interaction between iron and carbon atoms. The structure is stabilized by hydrogen bonds interactions involving oxygen

(55) Colacio, E.; Dominguez-Vera, J. M.; Lloret, F.; Moreno Sanchez, J. M.; Kivekäs, R.; Rodriguez, A.; Sillanpää, R. *Inorg. Chem.* **2003**, *42*, 4209.

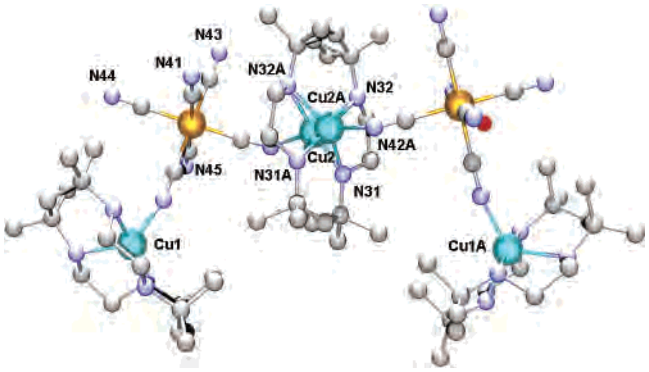

Figure 5. Perspective view of the pentanuclear structure of **6**: Fe^{III} (orange); Ni^{II} (green); N (blue); C (gray).

atoms of the disordered perchlorate anions and water molecules and NH groups of the *rac*-CTH macrocycle, leading to a 1D arrangement of squares.

[{Cu(*rac*-CTH)}$_3${Fe(CN)$_6$)}$_2$]·2H$_2$O (6). The structure of **6** (Figure 5) consists of cyanide-bridged pentanuclear [{Cu(*rac*-CTH)}$_3${Fe(CN)$_6$)}$_2$] molecules with C_2 symmetry and crystal water molecules involved in an intricate network of hydrogen bonds.

Within the pentanuclear molecules, three [Cu(*rac*-CTH)]$^{2+}$ units are alternatively bridged by two [Fe(CN)$_6$]$^{3-}$ anions, in which the cyanide-bridging groups adopt a cis configuration. The central [Cu(*rac*-CTH)]$^{2+}$ unit is disordered on two positions, because of the presence of both *RR* and *SS* enantiomers of the *rac*-CTH ligand coordinated to the copper(II) ion, Cu2. There is a 2-fold axis in the middle of the imaginary line between the disordered Cu2 ions, and therefore, bond distances and angles in the two halves of the pentanuclear molecule are equal. The Cu1 atoms of the terminal [Cu1(*rac*-CTH)]$^{2+}$ units exhibit a CuN_5 coordination environment with a geometry that is intermediate between square-pyramidal (C_{4v}) and trigonal bipyramid (D_{3h}). According to Addison's procedure,[56] the τ value for the Cu1 atom is 0.75 ($\tau = (\theta_1 - \theta_2)/60°$; where θ_1 and θ_2 are the two biggest angles in the coordination polyhedron; $\tau = 1$ for D_{3h}, and $\tau = 0$ for C_{4v}), thus indicating that the geometry of the Cu1 atom is closer to a trigonal bypiramid. In this description, two nitrogen atoms belonging to the macrocycle ligand (N1 and N4) occupy the axial positions, whereas the two remaining nitrogen atoms of the macrocycle and the nitrogen atom of the cyanide-bridging ligand are located in equatorial positions. The Cu1−N bond distances and cis N−Cu1−N angles are in the ranges 2.025(4)−2.139(5) Å and 84.44-(19)−119.9(2)°, respectively, whereas the N1−Cu1−N3 trans axial bond angle is 174.8(2)°.

The central copper(II) atom, which is disordered on two positions, displays a CuN_6 coordination environment, in which the four nitrogen atoms of the macrocycle occupy the equatorial positions, whereas the nitrogen atoms belonging to the cyanide bridging groups are in axial positions with a shortest Cu2−N distance of 2.305(10) Å. As usual, the [Fe(CN)$_6$]$^{3-}$ anions exhibit a slightly distorted octahedral geometry with Fe−C bond distances and cis and trans bond angles in the ranges 1.919(9)−1.952(7) Å, 87.0(3)−93.9-(3)°, and 176.1(3)−176.9(3)°, respectively. In the Cu1−NC−Fe bridging region, the Fe−C−N and C−N−Cu1 angles are 178.1(8) and 166.4(5)°, respectively, whereas the Fe···Cu distance is 5.084(8) Å. In the Cu2−NC−Fe bridging region, the Cu2−N−C bond angle is 139.5(9)° and the shortest Cu···Fe distances is 4.951(7) Å. The macrocycle amino groups N1−H, N3−H, and N4−H, the nitrogen atoms N44 and N45 of the terminal cyanide groups, and the water molecules are involved in an extensive network of hydrogen bonds leading to honeycomb layers in the *ab* plane with donor−acceptor distances in the range 2.890(7)−3.039(7) Å.

(56) Addison, A. W.; Burke, P. J.; Henrik, K. *Inorg. Chem.* **1982**, *21*, 60.

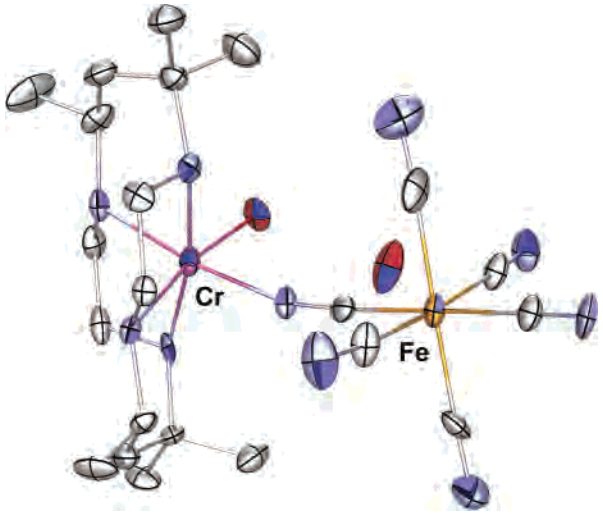

Figure 6. Perspective view of the dinuclear structure of **8**: Fe^{III} (orange); Cr^{III} (pink); N (blue); C (gray); O (red).

Although the compound [{Cu(*rac*-CTH)}$_3${Cr(CN)$_6$)}$_2$]·2H$_2$O (**7**) crystallizes in very well formed cube shaped crystals, it does not produce any diffraction peaks. Crystals from different syntheses exhibit the same diffraction behavior. Nevertheless, the analytical and IR results strongly suggest that compounds **6** and **7** are isostructural.

[Cr(*rac*-CTH)(H$_2$O)Fe(CN)$_6$]·2H$_2$O (8). The structure of **8** (Figure 6) consists of neutral $Fe^{III}Cr^{III}$ dinuclear molecules, [Cr(*rac*-CTH)(H$_2$O)Fe(CN)$_6$], and crystallization water molecules. Within the dinuclear unit, the [Fe(CN)$_6$]$^{3-}$ anion acts as a monodentate ligand to the Cr^{III} ion through a cyanide group. The Cr^{III} ion exhibits a distorted octahedral CrN_5O coordination environment, in which the nitrogen atom belonging to the cyanide bridging group and the oxygen atom of the coordinated water molecule are located in cis positions, whereas the remaining four coordination positions are occupied by the nitrogens atoms of the folded *rac*-CTH ligand. The Cr−N$_{macrocycle}$ bond distances are in the range 2.075(6)Å−2.138(6) Å, whereas the Cr−N$_{cyanide}$ and Cr−O bond distances are 1.999(6) and 1.989(5) Å, respectively. As for the hexacyanoferrate(III) unit, with the exception of the short Fe−C bond length of the cyanide bridging group (1.896(9) Å), the rest of the Fe−C bond distances exhibit normal values. In the bridging region, the Cr−N−C and Fe−C−N angles are 163.0(6) and 172.1(7)°, respectively, whereas the Cr···Fe distance is 4.9560(15) Å. The dinuclear molecules and water molecules form a complicated 3D

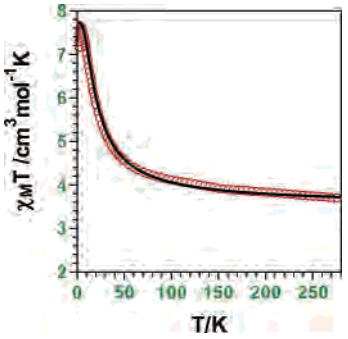

Figure 7. Temperature dependence of the $\chi_M T$ product of **2**. The solid line is the best-fit curve to the theoretical equation.

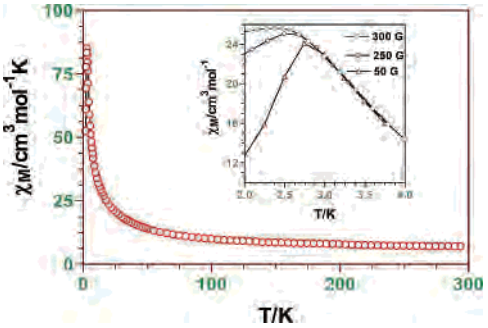

Figure 8. Temperature dependence of the $\chi_M T$ product of **3.** The inset represents the thermal variation of the susceptibility at different magnetic fields. The solid line is the best-fit curve to the theoretical equation.

network of hydrogen bonds, involving the NH groups of the macrocyclic ligand, the nitrogen atoms of the terminal cyanide groups, and the coordinated and noncoordinated water molecules. The shortest donor−acceptor distances of 2.597(8) and 2.640(8) Å involve the oxygen atom of the coordinated water molecule and the oxygen atoms of the noncoordinated water molecules.

Magnetic Properties. The temperature dependence of $\chi_M T$ (χ_M is the susceptibility/Fe_2Ni_2 unit at a magnetic field of 250 G) for compound **2** is given in Figure 7.

At room temperature the $\chi_M T$ product (3.66 cm^3 mol^{-1} K) is slightly higher than that calculated for magnetically noninteracting low-spin Fe^{III} ($S = 1/2$) and Ni^{II} ($S = 1$) ions of 2.75 cm^3 mol^{-1} K (with $g_{Fe} = g_{Ni} = 2$). From room temperature, $\chi_M T$ increases with decreasing temperature, reaching a maximum around 4 K (7.6 cm^3 mol^{-1} K) and further decreases to 7.16 cm^3 mol^{-1} K at 2 K. This behavior is characteristic of an overall ferromagnetic interaction leading to a septuplet ground state. The calculated value for an $S = 3$ ground state with $g = 2$ (7.81 cm^3 mol^{-1} K) is close to the $\chi_M T$ value at the maximum. The magnetization value at the maximum applied field of 5 T (5.67 $N\beta$) is close to the calculated value for a low-lying spin septet ($M_s = 6.0$ $N\beta$ with $g = 2$), thus supporting the nature of the ground state. As in **1**, the intramolecular ferromagnetic interaction is due to the strict orthogonality between $t_{2g}^5e_g^0$ Fe^{III} (σ symmetry) and t_{2g}^6eg2 Ni^{II} (π symmetry) magnetic orbitals. The decrease in $\chi_M T$ below 4 K is due to zero-field splitting effects within the ground state and/or intermolecular interactions. Simulation of the $\chi_M T$ vs T data using the MAGMUM program[57] with the spin Hamiltonian $H = -J[S_{Fe1}S_{Ni1} + S_{Fe1}S_{Ni2} + S_{Fe2}S_{Ni1} + S_{Fe2}S_{Ni2}]$ (all intramolecular exchange coupling constants along the edges were considered to be equal, whereas those along the diagonal were assumed to be zero) led to a $g_{iso} = 2.26(3)$ and $J_{FeNi} = 12.8(2)$ cm^{-1}. No improvement of the fitting was obtained using two independent J parameters. The magnitude of the exchange coupling between Fe^{III} and Ni^{II} via the −CN− linkage is higher than the literature values ranging from 6.6 to 10.6 cm^{-1}.[16b,c,18a,20b] Compared to **2**, the recently reported molecular square $[TpFe^{III}(CN)_3Ni^{II}(DMF)_4]_2(OTf)_2\cdot 2DMF$ exhibits a smaller ferromagnetic interaction (10.6 cm^{-1}), which is, in principle, difficult to justify as the Fe···Ni distances are similar in both compounds and the C−N−Ni angles in the bridging region are sharper for **2** than for $[TpFe^{III}(CN)_3Ni^{II}(DMF)_4]_2(OTf)_2\cdot 2DMF$ (the ferromagnetic interaction diminishes with the bending of the Cr−CN−Ni unit). It should be noted, however, that theoretical and experimental studies have shown that the change of the peripheral ligands in single-oxalate dinuclear complexes has a direct influence on the magnetic orbital energy and therefore on the magnitude of the magnetic exchange coupling.[59] The fact that Ni^{II} and Fe^{III} ions exhibit very different coordination environments in the molecular squares **2** and $[TpFe^{III}(CN)_3Ni^{II}(DMF)_4]_2(OTf)_2\cdot 2DMF$ might tentatively justify the difference in the J values for both compounds.

It is interesting to note that $[TpFe^{III}(CN)_3Ni^{II}(DMF)_4]_2(OTf)_2\cdot 2DMF$ shows slow magnetic relaxation effects and so single molecule magnet behavior with a blocking temperature lying below 1.8 K. Unfortunately, in the case of **2** no out-of-phase ac signal was observed, thus excluding the occurrence of slow magnetic relaxation. The compound does not exhibit SMM behavior probably because the zero-field splitting parameter, D, is either too small or positive.

The magnetic properties of **3** in the form $\chi_M T$ vs T plot (χ_M is the susceptibility/Cr_2Ni_3 unit at a magnetic field of 1 T) are given in Figure 8.

At room temperature, the $\chi_M T$ value of 6.90 cm^3 mol^{-1} K agrees well with that expected for magnetically noninteracting Cr^{III} ($S = 3/2$) and Ni^{II} ions (6.75 cm^3 mol^{-1} K with $g_{Cr} = g_{Ni} = 2$). The $\chi_M T$ increases smoothly between 300 and 50 K upon cooling and then sharply below 50 K, reaching a maximum of 85 cm^3 mol^{-1} K at 2.9 K. Further cooling causes a sharp decrease in $\chi_M T$ to reach a value of 52.4 cm^3 mol^{-1} K at 2 K. This magnetic behavior is indicative of an intrachain ferromagnetic interaction between Cr^{III} and Ni^{II} ions (strict orthogonality between the Cr^{III} t_{2g} magnetic orbitals of σ symmetry and the Ni^{II} e_g magnetic

(57) MAGMUN4.0/OW0L is available as a combined package free of charge from the authors at http://www.ucs.mun.ca/∼lthomp/. MAGMUN has been developed by Dr. Zhiqiang Xu and Laurence K. Thompson (Memorial University), and OW01.exe, by Dr. O. Waldmann (University of Bern). The software calculates the total spin state values (S') and their associated energies (E') using the Kambe approach[58] and then substitutes the S' and E' values into the van Vleck equation to generate the variable-temperature susceptibility profile (degenerate states are accounted for).

(58) Kambe, K. *J. Phys. Soc. Jpn.* **1950**, *5*, 48.

(59) Román, P.; Guzmán-Miralles, C.; Luque, A.; Beitia, J. I.; Cano, J.; Lloret, F.; Julve, M.; Alvarez, S. *Inorg. Chem.* **1996**, *35*, 3741.

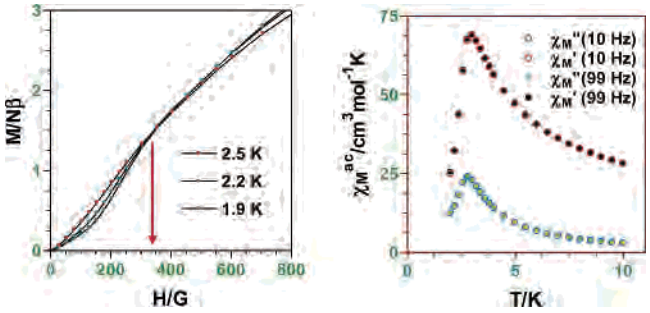

Figure 9. Isotherms of the magnetization versus H plot for **3** (left). Temperature dependence of the in-phase (χ_M') and out-of-phase (χ_M'') ac magnetic susceptibilities.

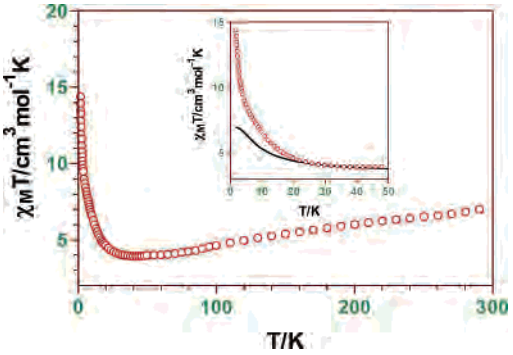

Figure 10. Temperature dependence of the $\chi_M T$ product for **4**. The inset is an expended view of the low-temperature region. The solid line is the generated plot for an Fe_2Ni_2 molecular square plus an isolated Cu(II) ion with $g = 2$.

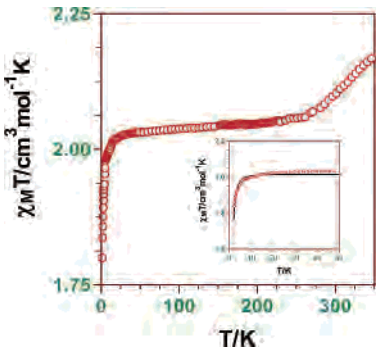

Figure 11. Temperature dependence of the $\chi_M T$ product for **5**. The inset is an expansion of the low-temperature region. The solid line is the best-fit curve to the theoretical equation for two isolated Ni^{II} ions with axial zero-field splitting.

orbitals of π symmetry) and suggestive of the existence of magnetic ordering. In-phase and out-of-phase ac dynamic susceptibility measurements (Figure 9) confirm the ferromagnetic ordering at 3 K. Because these signals do not show any significant frequency dependence of the position of the maximum, single-chain magnet behavior (SCM) for **3** can be ruled out. The absence of SCM behavior is more probably due to the fact that the chains are not well isolated in the structure (see above). The field dependence of the magnetization (0−5 T) measured at 1.9 K reaches a value of $M_s \approx 8.5\ N\beta$ at 5 T, which is smaller than the saturation value (M_0 ca. 12 $N\beta$) expected for a ferromagnetic Ni_3Cr_2 system ($M_0 = 3g_{Ni}S_{Ni} + 2g_{Cr}S_{Cr}$). This low value may be indicative of a canted ferromagnet which would be related to the fact that the planes of the Cr_2Ni_2 square units belonging to two adjacent chains make an angle of about 75°, assuming that the magnetic moment in each chain is perpendicular to the square plane. A similar magnetic behavior has been observed for compound **1**.

The χ_M vs T plot under an applied field of 50 G exhibits a maximum around 3 K, which is due to antiferromagnetic interchain interactions. This maximum broadens and disappears for $H > 300$ G (see inset Figure 8), and therefore **3** exhibits metamagnetic behavior (phase transition from an antiferromagnetic to a ferromagnetic ordered state induced by the magnetic field). The sigmoidal shape of the M vs T plot (see Figure 9, left) is the signature of the metamagnetic behavior. From the value of the critical field $H_c = 300$ G (the inflection point in Figure 9, left) a value of 0.03 cm^{-1} can be estimated for the magnetic interchain interactions. The lack of a theoretical model to analyze the magnetic data of **3** precludes the determination of the magnetic exchange interaction between Cr^{III} and Ni^{II}. Compound **3** is a metamagnet whereas **1** is a ferromagnet with $T_c = 3$ K. We think that subtle changes in the hydrogen bond networks of these compounds are responsible for their different magnetic behavior at low temperature.[19]

The magnetic properties of **4** in the form $\chi_M T$ vs T plot (χ_M is the susceptibility/Fe_2Ni_2Cu unit at a magnetic field of 1 T) are given in Figure 10.

The $\chi_M T$ product at room temperature is higher than that calculated for magnetically noninteracting Fe^{III}, Ni^{II}, and Cu^{II} ions (3.125 $cm^3\ mol^{-1}$ K with an average $g = 2$), thus indicating a significant orbital contribution from the octahedral low-spin Fe^{III} atoms. Upon cooling of the sample, $\chi_M T$ decreases to reach a minimum of 3.03 $cm^3\ mol^{-1}$ K at around 40 K, which is due to the spin−orbit coupling effects of the low-spin octahedral Fe^{III} atoms with a $^2T_{2g}$ ground term. Below 40 K, $\chi_M T$ increases sharply to a value of 11.14 $cm^3\ mol^{-1}$ K at 2 K. This behavior is indicative of an overall ferromagnetic interaction, which, as in the previous compounds, can be justified by the orthogonality of the t_{2g} magnetic orbitals of the low-spin Fe^{III} ions (π symmetry) and the e_g magnetic orbitals of the Ni^{II} and Cu^{II} atoms (σ symmetry). Nevertheless, because of the relatively long bond Cu−N distance (2.46 Å) and because the nitrogen atom of the cyanide-bridging ligand is coordinated at axial position on the copper atom, where the spin density of the unpaired electron is very low (the Cu^{II} atom is of the type $d_{x^2-y^2}$, the x and y axes being defined by the short $Cu-N_{cyclam}$ bonds), a very weak ferromagnetic interaction beetween the Fe^{III} and Cu^{II} ions, if any exists, can be predicted. The fact that the $\chi_M T$ values at low temperature are above those calculated for an isolated Fe_2Ni_2 molecular square plus the copper contribution (see inset Figure 10) clearly points out that some degree of spin correlation between the magnetic ions exists along the trimetallic chain.

The temperature dependence of $\chi_M T$ (χ_M is the susceptibility/Fe_2Ni_2 unit at a magnetic field of 1000 G) for **5** is given in Figure 11.

Upon cooling of the sample from 350 K, $\chi_M T$ first decreases, reach a quasi-plateau around 200 K, and finally sharply decreases from 50 to 2 K. The decrease in $\chi_M T$ in

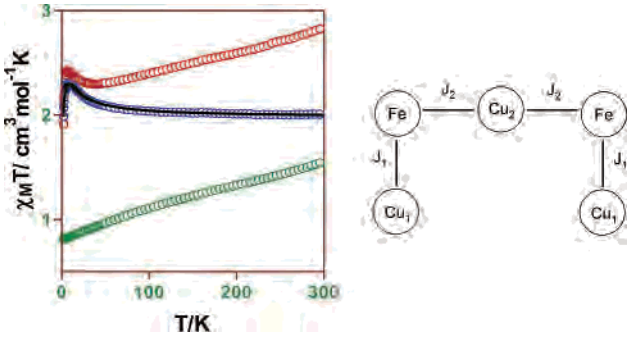

Figure 12. Temperature dependences of the $\chi_M T$ product of **6** (top), the corrected $\chi_M T$ product of **6** (middle), and the $\chi_M T$ product of (*rac*-$CTH_3)_3$-$[Fe(CN)_6]_2 \cdot 8H_2O$. The solid line is the best-fit curve to the theoretical equation for a linear pentanuclear Fe_2Cu_3 complex.

the high-temperature region (350−200 K) is due to the end of a transition from the high-spin to the low-spin state of the octahedral Fe^{II} ion. It should be noted that a similar HS:LS equilibrium has been observed in the 2D cyanide-bridged bimetallic compound, $Fe(bpy)_2(CN)_2Cu_2(CN)_2]$,[55] which, like **5**, also contains Fe^{II} atoms coordinated by two bpy and two cyanide ligands, leading to an FeC_2N_4 coordination environment. Recently, an Fe^{II} molecular square, $[Fe^{II}_4(CN)_4(bpy)_4(tpa)_4](PF_6)_4$ (tpa = tris(2-pyridylmethyl)amine), that undergoes two-step spin conversion of the Fe^{II} ions bonded to the tpa ligand has been reported.[18i] The transition observed in the range 240−400 K must also contain the end of the transition involving the Fe^{II} ions bonded to the bpy ligands. At 200 K, the $\chi_M T$ value (2.05 $cm^3\ mol^{-1}\ K$) is close to the calculated value for a magnetically uncoupled system with two low-spin Fe^{II} ions ($S = 0$) and two Ni^{II} ions ($S = 1$) assuming an average $g = 2$. The decrease in $\chi_M T$ from a value of 2.03 $cm^3\ mol^{-1}\ K$ at 50 K to 1.80 $cm^3\ mol^{-1}\ K$ at 2 K is due to the local anisotropy of the Ni^{II} ions. The $\chi_M T$ data can be well reproduced (inset Figure 11) by using the theoretical equation for two magnetically noninteracting Ni^{II} ions ($S = 1$) with axial zero-field splitting derived from the Hamiltonian $H = D[S_z^2 - 1/3S(S + 1)]$, where D is the energy difference between $M_s = \pm 1$ and $M_s = 0$ levels. The best fit leads to $|D| = 2.65(6)\ cm^{-1}$ (the sign of D cannot be determined from powder magnetic susceptibility data) and $g = 2.012(2)$. The D value is similar to those observed for other compounds containing Ni^{II} ions with distorted octahedral geometries.[60]

The magnetic properties of **6** in the form $\chi_M T$ vs T (χ_M is the magnetic susceptibility/Fe_2Cu_3 unit under an applied field of 1 T) are given in Figure 12.

In keeping with the orbital contribution of the low-spin Fe^{III} ion, at room temperature, the $\chi_M T$ product (2.84 $cm^3\ mol^{-1}\ K$) is higher than the calculated value for magnetically isolated low-spin Fe^{III} ($S = 1/2$, $g = 2$) and Cu^{II} ($S = 1/2$, $g = 2$) ions of 1.875 $cm^3\ mol^{-1}\ K$. $\chi_M T$ decreases upon cooling reaching a minimum value of 2.298 $cm^3\ mol^{-1}\ K$ at around 40 K (Figure 12, top). Such magnetic behavior is due, as in compound **3**, to the spin−orbit coupling within the $^2T_{2g}$ ground term of the low-spin octahedral Fe^{III} ion. In fact, when the $\chi_M T$ product between 40 K and room temperature for the compound (*rac*-$CTH_3)_3[Fe(CN)_6]_2 \cdot 8H_2O$[61] (whose magnetic properties are essentially due to isolated Fe^{III} ions of the $[Fe(CN)_6]^{3-}$ units) is subtracted from the $\chi_M T$ vs T curve for **6**, the resulting $\chi_M T$ remains almost constant in this temperature range with the value expected for three isolated Cu(II) ions with $g = 2.11$ of 1.246 $cm^3\ mol^{-1}\ K$. This result confirms that the magnetic behavior of **6** in the high-temperature range is due to spin−orbit coupling effects. Below 40 K, the $\chi_M T$ continuously increases to reach a maximum of 2.428 $cm^3\ mol^{-1}\ K$ at 7 K, thus indicating a ferromagnetic exchange interaction between the Fe(III) and Cu(II) ions. Below 7 K, $\chi_M T$ decreases sharply to 1.91 $cm^3\ mol^{-1}\ K$ at 2 K, due to intermolecular interactions and/or ZFS of the ground state. These factors are also responsible that the M vs H plot at 2 K is below that calculated from the Brillouin function with $S = 5/2$. At 5 T, the maximum applied magnetic field, the value of the magnetization is 4.14 $N\beta$, thus indicating that at this magnetic field the magnetization is not yet saturated ($M_s = 5\ N\beta$).

To analyze the experimental $\chi_M T$ data in a suitable way, we removed the contribution of the spin−orbit coupling effects of the three Fe^{III} ions. For this, we subtracted from the experimental $\chi_M T$ data of **6** those of the compound (*rac*-CTH-$H_2)_3[Fe(CN)_6]_2 \cdot 8H_2O$ and then the contribution of two isolated metal ions with $S = 1/2$ and $g = 2$ was added,

$$\chi_M T = \chi_M T\{[Cu(\text{rac-CTH})]_3[Fe(CN)_6]_2\} - \chi_M T(CTH_3)_3[Fe(CN)_6]_2 \cdot 8H_2O + 2\frac{Ng^2\beta^2}{4k}$$

As can be observed in the corrected plot (Figure 12, middle), upon cooling of the sample, $\chi_M T$ increases continuously from room temperature until reaching the maximum at 7 K. In keeping with the structural data for **6**, the corrected $\chi_M T$ data were analyzed using a five spin model (see Figure 12) through the isotropic spin Hamiltonian

$$H = -J_1(FeCu_1 + Fe_ACu_{1A}) - J_2(Fe_ACu_2 + FeCu_2) + g\beta H(S(Cu_1) + S(Cu_{1A}) + S(Cu_2) + S(Fe) + S(Fe_A))$$

in which the Cu−Cu and Fe−Fe exchange interactions have been neglected. The best fit of the data to the theoretical equation derived from the above Hamiltonian (a Θ parameter was included to take into account interpentanuclear interactions) yielded the following parameters: $J_1 = 13.8(2)\ cm^{-1}$, $J_2 = 3.9(4)\ cm^{-1}$, $g = 2.05(1)$, $\Theta = -1.3$ K. The

(60) Carlin, R. L. *Magnetochemistry*; Springer-Verlag: Berlin, 1986.

(61) This compound was prepared from the reaction between $K_3[Fe(CN)_6]$ (0.18 g, 0.55 mmol), *rac*-CTH (0.23 g, 0.82 mmol), and 1 mL of 2 M HCl (2 mmol) in a methanol/water mixture (1:1). After slow evaporation at room temperature, the compound crystallizes as yellow cubes. Yield: 63%. Crystallographic analysis ($C_{60}H_{130}Fe_2N_{24}O_8$): monoclinic, space group *Cc*; $a = 11.1482(10)$, $b = 18.2633(11)$, $c = 38.173\ (4)$ Å; $\beta = 92.706(11)°$; $V = 7763.5(12)$ Å^3; $Z = 4$; $\rho = 1.221$ g cm^{-3}; μ(Mo Kα) = 0.437 mm^{-1}; $F(000) = 1574$; $T = 153(2)$ K; Stoe Image Plate Diffraction System; Mo Kα radiation ($\lambda = 0.710\ 73$ Å); $2\theta_{max} = 52.1°$; 27 862 reflections measured, 14 326 of which were unique ($R_{int} = 0.1735$). The final refinement gave R = 0.0691 and wR = 0.1276 for 3667 observed reflections ($I > 2\sigma(I)$) and 848 variables. The structure consists of three *rac*-$CTH\text{-}H_2^{2+}$ cations, two $[Fe(CN)_6]^{3-}$ cations, and eight molecules of water, all of them involved in an intricate network of hydrogen bonds.

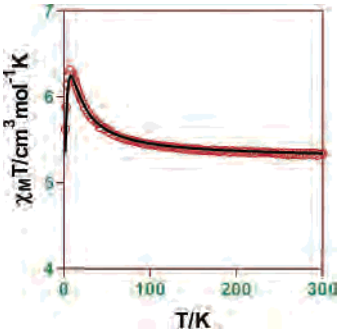

Figure 13. Temperature dependence of the $\chi_M T$ product of **7**. The solid line is the best-fit curve to the theoretical equation.

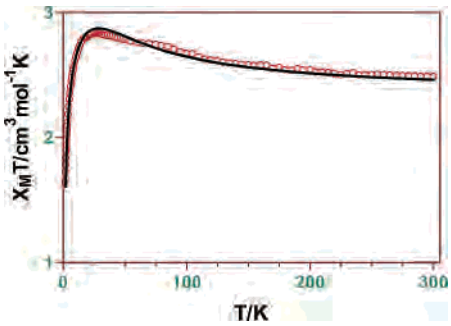

Figure 14. Temperature dependence of the $\chi_M T$ product of **8**. The solid line represents the best-fit curve to the theoretical equation.

ferromagnetic interaction between the Fe^{III} and Cu^{II} ions is a consequence of the orthogonality of their magnetic orbitals. The Cu1 ion, with a trigonal bpyramidal geometry, has a d_{z^2} magnetic orbital (directed toward two nitrogen atoms of the macrocycle) with mixture of the $d_{x^2-y^2}$ orbital, both of σ symmetry. The Cu2 ion, with an elongated octahedral geometry, has a $d_{x^2-y^2}$ magnetic orbital (directed toward the nitrogen atoms of the macrocycle) also of σ symmetry. The t_{2g} (d_{xy}, d_{xz}, and d_{yz}) magnetic orbitals of the low-spin Fe^{III} ion are, as indicated elsewhere, of π symmetry. Therefore, the interaction between orthogonal σ and π magnetic orbitals leads to the observed ferromagnetic interaction. Because the Cu2−N distance is rather long and because the nitrogen atom of the cyanide-bridging ligand is axially coordinated, the Fe^{III}/Cu_2^{II} magnetic exchange interaction is much weaker than the Fe^{III}/Cu_1^{II} one. The magnitude of the J_1 exchange coupling is similar to those observed for other cyano-bridged $Fe^{III}-Cu^{II}$ complexes with short N−Cu bond distances of about 2 Å, which are found in the range 8.6−12.6 cm^{-1}.[18b,c,62]

The temperature dependence of $\chi_M T$ (χ_M is the molar magnetic susceptibility/Cr_2Cu_3 unit under an applied field of 0.1 T) of **7** is given in Figure 13.

As it can be observed in this figure, the $\chi_M T$ increases continuously with decreasing temperature from a value of 5.34 cm^3 mol^{-1} K at room temperature until reaching a maximum of 6.23 cm^3 mol^{-1} K at 8 K and then decreases to a value of 5.37 cm^3 mol^{-1} K at 2 K. The increase in $\chi_M T$ is indicative of ferromagnetic interaction between the Cu^{II} and Cr^{III} ions, which is a consequence of the orthogonality of their magnetic orbitals, e_g (σ character) and t_{2g} (π character), respectively. The decrease in $\chi_M T$ below 8 K is due to either ZFS of the ground state or intermolecular antiferromagnetic interactions. Because **6** and **7** are isostructural, the magnetic data were analyzed with the same model. From the best fit to the calculated equation for the temperature dependence of the χ_M, the following parameters were obtained: $g = 2.08(1)$; $J_1 = 6.95(3)$ cm^{-1}; $J_2 = 1.9(2)$ cm^{-1}; $\Theta = -1.5(1)$ K. The J_1 exchange parameter falls in the range of values previously reported (6.0−45.5 cm^{-1}) for the exchange coupling between Cu^{II} and Cr^{III} through a cyanide bridge with short Cu−N distances of about 2 Å.[23,63]

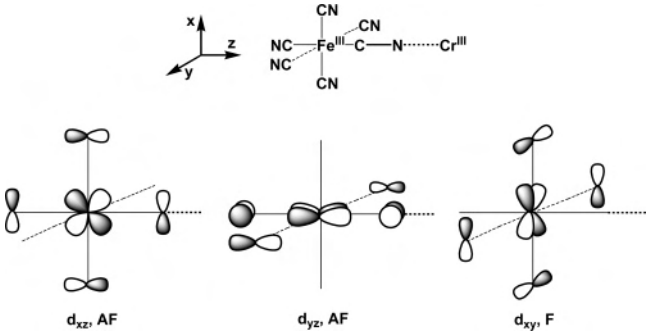

Figure 15. Schematic visualization of three possible magnetic orbital of the iron(III) mononuclear complex and the expected nature of the magnetic exchange coupling for each one of them with the magnetic orbitals of the chromium(III) ions in **8**. The labels F and AF are used to indicate ferro- and antiferromagnetic interactions.

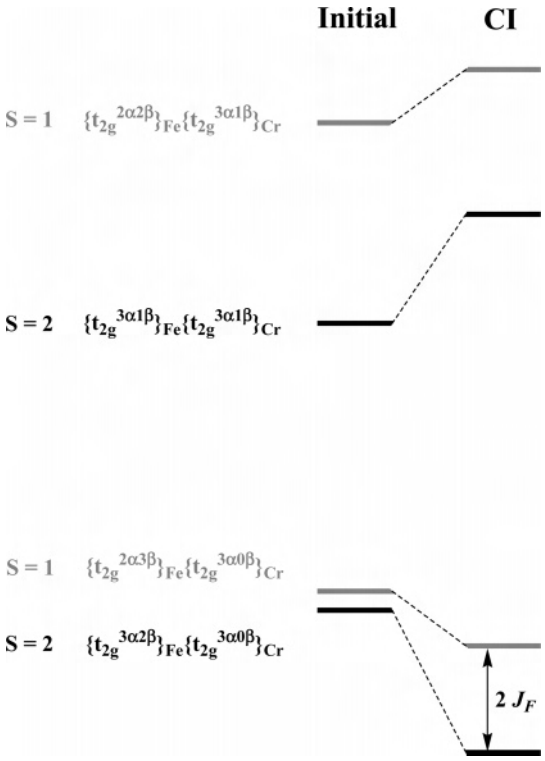

Figure 16. Qualitative energy diagram of the lower lying quintet and triplet states in **8** (black and gray, respectively). The notation of the electronic configurations indicates the number of α and β electrons on the t_{2g} orbitals of the iron(III) and chromium(III) ions. In the first (original) and second (CI) columns are displayed the expected order of the states and the order found after a configuration interaction was applied.

(62) Parker, R. J.; Lu, K. D.; Batten, S. R.; Moubaraki, B.; Murray, K. S.; Spiccia, L.; Cashion, J. D.; Rae, A. D.; Willis, A. C. *J. Chem. Soc., Dalton Trans.* **2002**, *19*, 3723.

Table 2. Atomic Spin Densities (in e^-) on Metal Ions in $[Fe(CN)_6]^{3-}$ and $[Cr(rac\text{-}CTH)(H_2O)]^{3+}$ Mononuclear Models and in the Complex **8**[a]

			$[Cr(rac\text{-}CTH)(H_2O)Fe(CN)_6]\cdot 2H_2O$ (**8**)			
			$S = 2$		$S = 1$	
param	$S = 1/2$ Fe for $[Fe(CN)_6]^{3-}$	$S = 3/2$ Cr for $[Cr(rac\text{-}CTH)(H_2O)]^{3+}$	Fe	Cr	Fe	Cr
ρ(d)[b]	1.051	2.997	1.385	2.663	−0.739	2.673
ρ(tot.)[c]	1.055	3.012	1.391	2.674	−0.743	2.685
$\Delta\rho$[d]			0.334	0.334	0.312	0.324

[a] In the last case results for quintuplet and triplet states are displayed. [b] Spin densities on d orbitals. [c] Total atomic spin densities on the metal ions. [d] Absolute value of number of the transferred electrons between metal ions in **8**, defined as the difference between the atomic spin densities (on d orbitals) in the complex **8** and in the corresponding mononuclear complex.

Figure 14 shows the temperature dependence of $\chi_M T$ for **8** under a magnetic field of 0.1 T.

With decreasing temperature, $\chi_M T$ increases gradually reaching a maximum of 2.835 $cm^3\ mol^{-1}$ K at 27 K, which is indicative of the presence of a ferromagnetic interaction between the Cr^{III} and Fe^{III} ions through the cyanide bridging group. Below 27 K, $\chi_M T$ decreases sharply to 1.63 $cm^3\ mol^{-1}$ K at 2 K as a consequence of either antiferromagnetic intermolecular interactions or ZFS effects of the $S = 2$ ground state. The M vs H plot at 2 K is below that calculated for the Brillouin function with $S = 2$, which is due to the ZFS and/or the antiferromagnetic interactions occurring at very low temperature. At 5 T, the value of the magnetization of 3.6 $N\beta$ is close to the magnetization saturation value of 4 $N\beta$ with $g_{mean} = 2$. To evaluate the exchange coupling between Cr^{III} and Fe^{III} ions through the CN bridge, the magnetic susceptibility data were fitted to the calculated equation derived from the Heisenberg Hamiltonian, $H = -JS_{Cr}S_{Fe}$. A Θ parameter was included to take into account intermolecular interactions. The best fit affords magnetic parameters of $g = 2.04(3)$, $J_1 = 28.87(3)$, and $\Theta = -1.9$ K. The Θ value may be overestimated because the ZFS of the ground state has not been taken into account in the theoretical equation.

In principle, the ferromagnetic coupling between Cr^{III} and Fe^{III} ions is hard to explain. If both metal ions were in an idealized O_h geometry, the interaction between their magnetic orbitals of t_{2g} type (π character) would lead to a good overlap and so to antiferromagnetic interactions. However, if the geometry of the metal ions is far from O_h, as in the case of **8**, the symmetry would decrease and then the magnetic orbitals would not still be degenerate. In this situation, ferromagnetic interactions might be observed. The same argument was invoked to explain the ferromagnetic interaction observed for the 1D chain complexes [M(cyclam)][Fe(CN)$_6$] (M = Mn^{III} and Fe^{III}).[64] To justify the sign and magnitude of the magnetic exchange interaction observed for **8**, DFT type calculations were carried out on this system.

In the chromium(III) ion the three t_{2g} orbitals act as magnetic orbitals, whereas in the low-spin iron(III) ion its five d electrons must be placed in three t_{2g} orbitals, only one of them being the magnetic orbital. Thus, the nature of the magnetic exchange coupling in **8** is governed by the spatial disposition of the magnetic orbital on the iron(III) ion. To simplify a qualitative analysis on the basis of the molecular orbitals, we have considered an ideal geometry where the z-axis is defined along the Fe−CN−Cr direction. In this description, antiferromagnetic contributions can be expected when the magnetic orbital on iron is the d_{xz} or the d_{yz} (Figure 15). Nevertheless, when the d_{xy} orbital is the magnetic orbital on the low-spin iron(III) ion, there is no delocalization from this magnetic orbital to the cyanide bridging ligand but to peripheral cyanide ligands. Therefore, the overlap with the magnetic orbitals of the chromium(III) is nil (Figure 15) and consequently a weak ferromagnetic contribution should be observed. However, the experimental results suggest a moderate ferromagnetic exchange coupling between the chromium(III) and low-spin iron(III) ions.

To find an explanation to this disagreement in the magnitude of the exchange coupling, we have carried out calculations of the electronic structure on the basis of the density functional theory. In previous works with cyano-bridged systems, we have observed that density functional calculations provide a good qualitative evaluation of the exchange coupling constants. However, from a quantitative point of view, the calculated magnetic couplings are overestimated.[41−44] In this respect, we have concluded that the presence of the charged terminal cyanide ligands is responsible for both the incorrect convergence of calculations and the overestimation of the exchange coupling constants. In fact, in these systems we have found different configurations closer in energy, being not an easy task to obtain the more stable configuration. Some approaches have been used to minimize both problems. Although the substitution of cyano groups by ammonia ligands minimizes both problems, it is not enough and occasionally other problems related to the influence of the terminal ligands can be joined.[41−44] The addition of a dielectric continuum to simulate the electronic influence of the solid on the molecule can improve the electronic description of peripheral cyanide ligands. The experimental dielectric constant in this kind of solid takes values between 5 and 10. Thus, we have chosen the dielectric constant of the solvent dichloromethane to simulate the solid effects. Our first calculations have been made on the mononuclear models built from the experimental geometry of **8**. The NBO analysis in the chromium(III) mononuclear ($S = 3/2$) shows that delocalization and polarization of the

(63) (a) El Fallah, M. S.; Ribas, J.; Solans, X.; Font-Bardia, M. *New J. Chem.* **2003**, *27*, 895. (b) Marvaud, V.; Decroix, C.; Scuiller, A.; Guyard-Duhayon, C.; Vaissermann, J.; Gonnet, F.; Verdaguer, M. *Chem.*—Eur. J. **2003**, *9*, 1677.

(64) (a) Colacio, E.; Domínguez-Vera, J. M.; Ghazi, M.; Kivekäs, R.; Lloret, F.; Moreno, J. M. *Chem. Commun.* **1998**, *10*, 1071. (b) Lijima, S.; Honda, Z.; Koner, S.; Mizutani, F. *J. Magn. Magn. Mater.* **2001**, *223*, 16. (c) Bhattacharjee, A.; Miyazaki, Y.; Nakazawa, Y.; Koner, S.; Lijima, S.; Sorai, M. *Physica B* **2001**, *305*, 56.

spin density on the carbon and nitrogen atoms of the cyanide groups, respectively,[65] are weak. In the same way, in the low-spin iron(III) mononuclear ($S = 1/2$) weak delocalization and polarization on the second (nitrogen) and first (carbon) neighbor atom of cyanide group are observed. In both cases, the spin density is placed almost on the metal ions, specifically in d orbitals, where it is near to the expected value for a free ion [3 and 1 e^- for the chromium(III) and iron(III) ions, respectively (see Table 2)].[65]

The calculations shows that the more stable configuration for the iron(III) mononuclear complex is that in which the magnetic orbital is the d_{xy} one. This result is also confirmed in theoretical calculations on **8**. Thus, according to the previous qualitative analysis, a weak ferromagnetic or nil exchange coupling is expected. However, the exchange coupling constant evaluated from energies calculated for the quintet and triplet states of **8** is $+35$ cm^{-1} ($+1480$ cm^{-1} in absence of the continuum model). This value is in agreement with that found from the experimental measurements. A detailed study on the atomic spin densities reveals partial charge transfers are the cause of the moderate magnetic coupling. In previous work, we have found that partial charge transfer has an important influence in the magnitude and nature of the magnetic exchange coupling.[66] In both states the charge transfer occurs from the iron(III) to the chromium(III) ion. Thus, in the quintet state the chromium(III) ion cannot accept an electron in its α t_{2g} orbitals and only the β t_{2g} electron of iron(III) can be transferred to the chromium (Figure 16). This fact is equivalent to consider an interaction or mixture between the $Fe^{III}Cr^{III}$ ground and the $Fe^{IV}Cr^{II}$ excited configurations (Figure 16). A similar situation is proposed for the triplet-BS configuration. In a semiquantitative way, the transferred electrons ($\Delta\rho$) have been calculated from the atomic spin densities in quintet- and triplet-BS states of **8** and those previously obtained in the mononuclear models (Table 1). In according to the abovementioned details, the electron charge transfer is observed in the quintet and triplet states. Despite the similarity between the schemes of the quintet and triplet states, there is a crucial difference. In the quintet- and triplet-BS states, the local electronic configurations of iron(IV) in the excited states are different. In the first case the iron(IV) is visualized as a triplet while in the last one it is done as a less stable singlet. Thus, it is expected a larger mixture between the ground and the excited configurations in the quintet state (Figure 16). This conclusion is supported by the $\Delta\rho$ values displayed in Table 1. In this sense, the quintet state becomes more stable than the triplet state and an increase in the magnitude of the ferromagnetic exchange coupling is observed.

(65) Cano, J.; Ruiz, E.; Alvarez, S.; Verdaguer, M. *Comment Inorg. Chem.* **1998**, *20*, 27.

(66) Carrasco, R.; Morgenstern-Badarau, I.; Cano, J. *Chem. Commun.* **2003**, *3*, 436.

Conclusions

$[M'(rac\text{-CTH})]^{n+}$ complexes ($M' = Cr^{III}$, Ni^{II}, Cu^{II}) with two cis available coordination positions, when assembled with cyanometalates, give rise to a rich variety of neutral cyano-bridged heterometallic complexes that exhibit $M^{II}_3M^{III}_2$ and $M^{III}M^{III}$ stoichiometries. The $[Ni(rac\text{-CTH})]^{2+}$ complex is an appropriate building block to obtain isolated molecular squares, which, if they have free cyanide groups, can be used as "ligands" toward trans planar $[M(macrocyle)]^{2+}$ ($M = Ni^{II}$ and Cu^{II}) to produce mixed ligands and trimetallic chains made of squares units. When the complexes $[Cu(rac\text{-CTH})]^{2+}$ and $[Cr(rac\text{-CTH})]^{3+}$ are used, only open structures can be obtained. This fact is due, in the first case, to the plasticity and Jahn−Teller effect of the Cu^{II} ion and, in the second case, to the coordination of a water molecule to the Cr^{III} ion that avoids the formation of the cyclic structure. This rational synthetic strategy can be extended to the assembly of other cyanometalate and anisotropic $[M(rac\text{-CTH}]^{n+}$ precursors, which should lead to new magnetic systems with potential SMM and SCM behaviors.

The different structures for complexes **2**−**8** have indeed afforded various magnetic behaviors (ferromagnet, metamagnet, spin crossover, etc.), which, in some cases, are significant for understanding the relation between structure and magnetic properties in cyano-bridged polynuclear systems. It is interesting to note the unexpected ferromagnetic interaction between Fe^{III} and Cr^{III} in compound **8**. The nature and magnitude of this magnetic interaction has been justified by DFT type calculations.

Acknowledgment. This work was supported by the Spanish Ministerio de Ciencia y Tecnología through Projects BQU2001/3221 and Junta de Andalucía. A.R.-D. thanks the Ministerio de Ciencia y Tecnología for a predoctoral fellowship.

Supporting Information Available: Crystallographic data in CIF format. This material is available free of charge via the Internet at http://pubs.acs.org.

IC061187J